AN INVESTIGATION OF THE BOUNDARY LAYER OF AN ATMOSPHERIC MESOSCALE VORTEX

axisymmetric

Gandikota V. Rao and William H. Raymond
Saint Louis University
Department of Earth and Atmospheric Sciences
St. Louis, Missouri 63103

Final Report
1 July 1975 - 31 August 1977

NATIONAL SEVERE STORMS LABORATORY
U.S. DEPARTMENT OF COMMERCE
NATIONAL OCEANIC AND ATMOSPHERIC ADMINISTRATION
NORMAN, OKLAHOMA 73069

AN INVESTIGATION OF THE BOUNDARY LAYER OF AN AXISYMMETRIC MESOSCALE VORTEX

PART I: THE EFFECT OF LOWER BOUNDARY CONDITIONS ON THE BOUNDARY LAYER STRUCTURE

by

G. V. Rao and W. H. Raymond
Dept. of Earth and Atmospheric Sciences
Saint Louis University

TABLE OF CONTENTS

ABSTRACT

The effect of the lower boundary conditions in modifying the boundary layer structure of an axi-symmetric, quasisteady maintained vortex is studied by extending the earlier investigation of Kuo (1971). Nonzero vertical velocities at the top of the sublayer representing the lower extremity of a vortex are prescribed. Positive values of vertical velocity signified pumping; negative, sucking. The two second order ordinary differential equations governing the tangential and radial velocities of the vortex are solved by employing a Newton's iterative method (Keller, 1968).

The result, namely that pumping elevates the boundary layer and destabilizes the motion and suction depresses the boundary layer and produces stability, confirmed the earlier finding of certain fluid dynamicists. Modifications of the boundary layer structure produced by spatially varying the angular momentum distribution of a vortex are analogous to those caused by the imposition of the Taylor boundary condition at the lower extremity of the vortex. They are also similar to those rendered by varying pumping or suction. The latter result is believed to be new while the former simply confirms an earlier theoretical deduction.

1. INTRODUCTION

The atmospheric vortices in general belong to various space and time scales. Those classified under the mesoscale category are being increasingly studied recently. A cause for this accelerated activity lies in the current demand for knowledge of the severe local storms and tornadoes which appear to develop intense vortical circulations and strong horizontal and vertical velocities. Since direct measurement of the motion field associated with these storms is very dangerous, reliance is placed on remote sensing. For a documentation of the vortical structure employing dual doppler radar see Ray (1976) and Brandes (1977). It is generally believed that these vortices are maintained through thermal convection. The means of maintenance is not of interest in this study. The velocity field above the boundary layer is characterized in general by the tangential field and a quasi-cyclostrophic balance appears to exist in the near steady state. Within the boundary layer the velocity distribution is different because of friction. Significant radial velocities and pronounced convergence fields are developed in the boundary layer. Because of lack of adequate velocity measurements in this layer the amount of convergence and its spatial distribution are not properly known. Recent radar observations, however, reveal that convergence attains its maximum values in the lowest few hundred meters (Ray, 1976). In addition to this 'normal' convergence mesovortices appear to develop sudden increases in the convergence field. This

abnormal convergence be it due to an explosive growth of convection pertaining to the mesovortex (Fujita and Caracena, 1977) or due to scales of motion larger than the mesovortex itself culminates in the production of large vertical velocities at lower elevations. In a laboratory such a process can easily be simulated by injecting mass through the bottom boundary— this process being termed blowing (e.g., Sparrow and Gregg, 1960) or pumping. The principal purpose of this article is to allow pumping* or suction to take place at the lower extremity of an idealized atmospheric vortex (radius about 5 km) and to examine the modified boundary layer structure. Pumping is included by prescribing positive values of vertical velocity and sucking by negative ones at the top of the surface layer.

Several earlier scientists had experimented with various types of lower boundary conditions, e.g., Eliassen (1971), Kuo (1971) and Bode, Leslie and Smith (1975) discussed the difference between the boundary layer structures with the slip and no-slip boundary conditions; Stuart (1954), Rogers and Lance (1960), Sparrow and Gregg (1960), Evans (1969), and Nguyen et al., (1975) found out that suction stabilizes the momentum field while Sparrow and Gregg (1960), Watson (1966), Kuiken (1971), Debnath and Mukherjee (1973) and Nguyen et al., (1975) observed that pumping causes a deepening of the boundary layer and hastens the transition from laminar flow

---

*The term 'blowing' was used instead of 'pumping' by certain scientists, e.g., Sparrow and Gregg (1960).

to turbulent thus contributing to an evantual destabilizing of the fluid flow.

The boundary layer of a local atmospheric vortex is undoubtedly very complex and its study through theoretical means is possible only after making several simplifying assumptions. Results based on such idealizations are still considered to be worthy if they provide valuable insights into the basic dynamics of the vortex.

2. THEORY

a. General Remarks

Several theoretical studies of the boundary layer of a vortex appeared in the literature. For a discussion and review of these see Schlichting (1968) and Davies-Jones and Vickers (1971). Modeling was done of a vortex in rigid rotation, e.g., Boedewadt (1940), or of a potential vortex, e.g., Burggraf et al., (1971), and Serrin (1972). Others have studied flows which vary from solid rotation near the inner core to potential far away from the center; e.g., Mack (1962), and King and Lewellen (1964) assumed the external tangential velocity to vary as $V \sim r^n$ where n varied from -1 to 1. A single value of

cannot describe the velocity distribution within the vortex. Chi (1974) considered a combined Rankine vortex and numerically integrated the governing equations for various Reynolds numbers.

In the following the structure of the boundary layer of a vortex subjected to both laminar and turbulent conditions, and in a quasisteady state having both solid and nonsolid rotation will be investigated. The vortex is assumed to have an inner core with rigid rotation. Studies by Rogers and Lance (1964), Rott and Lewellen (1964), and Chi (1974) tend to confirm this assumption. Following Kuo (1971) non-rigid rotation is modeled away from this inner core by a power law representation of the momentum distribution. It is well known that such an idealized structure will not yield solutions that represent either potential or near potential flow, e.g., see Kuo (1971), King and Lewellen (1964), or Burggraf et al.,

(1971). Nevertheless the assumption of a power law variation of momentum is sufficient for our purposes because the variations between laminar and turbulent flows are most pronounced within the interior of a concentrated vortex (see also Bode et al., 1975).

b. Relevant Equations

In this investigation Kuo's (1971) study of the boundary layer of an axisymmetric vortex is followed and the governing Navier-Stokes equations are formulated by assuming that variations along the boundary are much smaller than variations normal to the boundary. Representing dimensional variables with a bar and denoting nondimensional variables by ordinary letters we set

$$\bar{v} = V_m v \; ; \quad \bar{u} = V_m u \; ; \quad \bar{w} = w V_m \delta_R r_m^{-1} \; ;$$
$$\bar{p} = \rho V_m^2 \tilde{p} \; ; \quad \bar{r} = r_m r \; ; \quad \bar{z} = \delta_R z \quad \text{and}$$
$$\bar{\nu} = \nu V_m \delta_R^2 r_m^{-1}$$

where V_m, r_m and δ_R are the maximum tangential velocity, a horizontal scale length and a reference boundary layer thickness, respectively. Some typical mesometeorological magnitudes of V_m, r_m, etc., are given in Appendix B. The governing nondimensional equations are:

$$u \frac{\partial u}{\partial r} + w \frac{\partial u}{\partial z} - \frac{v^2}{r} = -\frac{\partial p}{\partial r} + \nu \frac{\partial^2 u}{\partial z^2} , \qquad (2.1)$$

$$u \frac{\partial v}{\partial r} + w \frac{\partial v}{\partial z} + \frac{uv}{r} = \nu \frac{\partial^2 v}{\partial z^2} , \text{ and} \qquad (2.2)$$

$$\frac{\partial u}{\partial r} + \frac{u}{r} + \frac{\partial w}{\partial z} = 0. \qquad (2.3)$$

The above are simplified by making use of the following similarity transformations (Kuo, 1971):

$$z = \delta\eta\,; \quad \partial p/\partial r = r^{4n-3}\,; \quad u = -r^{2n-1}F(\eta)\,; \quad v = r^{2n-1}G(\eta)$$

$$w = \left[(n+1)H(\eta) + (n-1)\eta F(\eta)\right] r^{n-1}\nu^{1/2} \text{ and } \delta = \nu^{1/2} r^{1-n}.$$

These transformations can be related to the angular momentum m through $v = m/r = m_o G/r$ and $u = -m_o F/r$, where $m_o = r^{2n}$. The boundary layer structure of different parts of the same vortex can be studied by letting n take several values in the range 1 to 0 thereby representing the flow from rigid rotation (n = 1) near the axis to the well known 'potential' vortex relationship outside the region of maximum winds (n = 0). However, as pointed out before, e.g., by Kuo (1971), mathematically speaking solutions for laminar flow do not exist for n much less than 0.5.

Utilizing the above similarity transformations Eqs. 2.1, 2.2 and 2.3 respectively become

$$\frac{d^2F}{d\eta^2} = (1-2n)F^2 + (n+1)H\frac{dF}{d\eta} + G^2 - 1\,, \tag{2.4}$$

$$\frac{d^2G}{d\eta^2} = (n+1)H\frac{dG}{d\eta} - 2nFG\,, \tag{2.5}$$

$$F = \frac{dH}{d\eta}\,. \tag{2.6}$$

c. Boundary Conditions

F, G and H can be obtained by solving the above system under proper boundary conditions. At a point δ_η located much higher than the customary top of the boundary layer the

Radial motion vanishes and cyclostrophic balance prevails, i.e., at

$$\eta = \delta_\eta \ , \quad F = 0 \quad \text{and} \quad G = 1. \tag{2.7}$$

At the lower extremity, $\eta = 0$, imposition of the no-slip boundary condition for laminar flow yields

$$F = G = H = 0. \tag{2.8}$$

For turbulent flow regimes a sublayer develops close to the surface within which velocity components decrease to zero. At the top of the sublayer, δ_b, velocity components are non-zero and are given by

$$V = K \, dV/d\eta \tag{2.9}$$

a relationship originally proposed by Taylor (1915) which is called the slip boundary condition or the geophysical boundary condition. Kuo (1971) regards K as a measure of the effective thickness of the sublayer δ_b. One can move the lower extremity from the surface to δ_b and propose the following conditions* there:

$$\text{at } \eta = \delta_b \ , \quad F = K \frac{dF}{d\eta} \ , \quad G = K \frac{dG}{d\eta} \quad \text{and} \quad H = h_o \tag{3.0}$$

---

* Alternatively, new variables

$\tilde{w} = h_o w$, and

$\zeta = \eta / h_o$, $h_o > 0$ are defined, following Kuiken (1971), and Eqs. 2.4 through 2.6 are transformed correspondingly. The second order terms $d^2F/d\eta^2$ and $d^2G/d\eta^2$ become respectively $h_o^{-2} d^2F/d\zeta^2$ and $h_o^{-2} d^2G/d\zeta^2$ thus pointing out the fact that the fluid behaves as though it is inviscid for large h_o's.

where h_o is a measure of the vertical velocity induced by the external divergence or convergence field. Positive values of h_o signify pumping and negative sucking. In the following since no detailed calculation of the velocity field is made in the sublayer the point $\eta = \delta_b$ is taken as $\eta = 0$ and the computations are performed in the interval $\eta = 0$ to δ_η.

Before the numerical solution of Eqs. 2.4, 2.5 and 2.6 is discussed, an analytical treatment, parallelling Kuo's development, is given so as to provide an insight into the role of pumping in altering the boundary layer structure of a vortex.

d. Analytical Solutions for Arbitrary Exponents, n's

Following Kuo (1971) let the Eqs. 2.4, 2.5 and 2.6 be expressed in terms of the new variables y, f and h through the relationships

$$\eta = n^{-1/4} y \; ; \quad H = n^{-3/4} h \quad \text{and} \quad F = n^{-1/2} f \quad \text{so that}$$

$$\frac{d^2 f}{dy^2} = a_1 h \frac{df}{dy} + a_2 f^2 + G^2 - 1 \, , \tag{3.1}$$

$$\frac{d^2 G}{dy^2} = a_1 h \frac{dG}{dy} - 2 fG \, , \tag{3.2}$$

$$f = \frac{dh}{dy} \tag{3.3}$$

where

$$a_1 = 1 + n^{-1} \quad \text{and} \quad a_2 = n^{-1} - 2 \, .$$

Further simplifications are made by expanding the flow variables in terms of a small number ϵ:

$$G = 1 + \sum_{j=1}^{\infty} \epsilon^j g_j \quad , \quad f = \sum_{j=1}^{\infty} \epsilon^j f_j$$

and

$$h = h_0 + \sum_{j=1}^{\infty} \epsilon^j h_j \tag{3.4}$$

where

$$h_j = \int_0^{\eta} f_j \, d\eta .$$

The appropriate boundary conditions are:

at y = 0

$$f_j = K^* \frac{df_j}{dy} \, , \quad j \geq 1 ,$$

$$g_{j+1} = K^* \frac{dg_j}{dy} \, , \quad j = 1 , \tag{3.5}$$

$$g_j = K^* \, dg_j/dy \, , \quad j > 1 \text{ and}$$

as $y \to \infty$

$$f_j = 0 \, , \quad j \geq 1 \, , \tag{3.6}$$

$$g_j = 0 \, , \quad j \geq 1 .$$

Here K^* is a small constant determined from (2.9) and the relationships governing η, y, H, h, F and f.

Substituting Eq. 3.4 into Eqs. 3.1 and 3.2 yields

$$\frac{d^2 f_j}{dy^2} - c\frac{df_j}{dy} - 2g_j = \sum_{i=1}^{j-1} \left(a_1 h_{j-i} \frac{df_i}{dy} + a_2 f_{j-i} f_i + g_{j-i} g_i\right)$$

$$\frac{d^2 g_j}{dy^2} - c\frac{dg_j}{dy} + 2f_j = \sum_{i=1}^{j-1} \left(a_1 h_{j-i} \frac{dg_i}{dy} - 2 f_{j-i} g_i\right)$$

where $c = a_1 h_o$.

Utilizing standard methods (Wylie, 1966) the solution of the homogeneous system associated with $j = 1$ is found to be

$$f_1 = (-a \sin qy + b \cos qy) \exp py \tag{3.7}$$

$$g_1 = (a \cos qy + b \sin qy) \exp py \tag{3.8}$$

$$h_1 = (p^2+q^2)^{-1} \left[\{(-ap+bq)\sin qy + (aq+bp)\cos qy\} \exp py - aq - bp \right] \tag{3.9}$$

where p and q are the real and imaginary parts, respectively of the complex roots $s = p + iq$ of the 4th degree characteristic equation

$$s^4 - 2cs^3 + c^2 s^2 + 4 = 0 \tag{4.0}$$

which leads to the identities

$$p^2 - q^2 - cp = 0 \quad \text{and} \quad |2pq - cq| = 2.$$

Because our solutions are bounded as $y \to \infty$ we can only accept roots for which $p \leq 0$. The values for a and b are determined for

$$a = -(1 - pK^*)\left(q^2K^{*2} + (1 - pK^*)^2\right)^{-1}$$

and

$$b = K^*q\left(q^2K^{*2} + (1 - pK^*)^2\right)^{-1}.$$

In Table 1 both the real (p) and the imagary term (q) of the roots of the characteristic equation are shown for various values of n and h_o. For the same n increased values of h_o cause reduction in the magnitude of p. An examination of the solutions (3.7, 3.8 and 3.9) then implies that the depth of the boundary layer is increased by pumping. Another important finding is that increasing h_o or decreasing n produces similar solutions. Thus pumping has the same effect on the results as decreasing n. For suction (results not presented) the magnitudes for p are larger than one and consequently this increased damping causes a reduction in the boundary layer thickness. These conclusions, valid for the first term of the analytical solution, can now be compared against the numerical answers of the nonlinear equations.

TABLE 1. Roots of the Characteristic Equation (4.0) for Various Values of n and h_o. (Note that increasing h_o has an effect on the roots similar to lowering n)

	← h_o → 0.0		0.2		0.4		0.6	
n (exponent in the power law)	(REAL)	(IMG.)	(REAL)	(IMG.)	(REAL)	(IMG.)	(REAL)	(IMG.)
1.0	-1.00	1.00	-.810	.990	-.641	.961	-.494	.914
0.75	-1.00	1.00	-.780	.987	-.589	.949	-.429	.886
0.50	-1.00	1.00	-.7227	.978	-.494	.914	-.318	.821
0.25	-1.00	1.00	-.564	.940	-.272	.786	-.122	.617
0.10	-1.00	1.00	-.232	.751	-.045	.448	-.014	.302
0.05	-1.00	1.00	-.051	.465	-.007	.238	-.002	.159

3. RESULTS

The fields of F, G and H from the numerical solutions of Eqs. 2.4, 2.5 and 2.6 are presented in Figs. 1-8 for various combinations of n, K, pumping and suction. Details of the numerical procedures are described in Appendix A. To limit the number of figures profiles of F which illustrate the boundary layer structure vividly are shown more than either G or H profiles. Corresponding dimensional quantities are obtained by referring to Table 2 in Appendix B.

Solutions with pumping (h_o= .2) and suction h_o= -.2) are contrasted against neutral (h_o=0) conditions in Fig. 1, which show the vertical profile of the radial component for laminar flow (K=0) in solid rotation (n=1). Pumping enhances the flow and increases the boundary layer thickness where as suction subdues the motion and decreases the boundary layer depth. These conclusions remain valid even when Taylor lower boundary conditions are used. For example, Fig. 2 shows similar findings when K=1.0. The ordinate of Figs. 2 through 7 is plotted only up to 10 although the computation was done through 20. From Figs. 3, 4 and 5 we see that by varying selected values of K, n and h_o, respectively, profiles that resemble each other result. In Fig. 3, n is fixed at 0.5 (nonsolid rotation) and K varied between 1.0 and 3.0. (The value K=1.7838109 was selected for comparison purposes because it is equivalent to the value of K = 1.5 when n=.5 in Kuo's study and in our analytical solution presented in Eqs. 3.7, 3.8 and 3.9.) These profiles

are very similar to those shown in Fig. 4 when K was held fixed and n varied between 0.35 and 0.75. Varying the lower boundary condition for H produces a similar effect on the F-field as is evident from Fig. 5. Thus, the previous conclusion (Section 2d), namely, enhanced pumping is equivalent to reducing n or decreasing K, also holds good on the basis of nonlinear solutions. In other words the externally induced vertical motions at the lower extremity tend to make a rigidly rotating vortex into a nonrigidly rotating one.

Figures 5, 6 and 7 show the typical effect of pumping and suction upon the dimensionless measures of radial, tangential and vertical velocities respectively. The F and H fields experience the most changes because of pumping or suction. Their respective maximum values in the low levels increased by as much as 25% and 60% over their neutral counterparts. The tangential velocity component G tends to be less effected.

Figure 8 shows that pumping has a substantial impact for the case n = 0.25 and K = 2. Burggraf and Stewartson (1975) have shown that as n is decreased the similarity solutions (F) approach a form reminiscent of a ladder and consequently do not want to satisfy the upper boundary conditions. Pumping, as pointed out before, is equivalent to reducing K or decreasing n. Thus, the situation described by Burggraf and Stewartson can occur in the presence of pumping for much larger values of n and/or K than previously suspected.

In Table 2 given in Appendix B, a set of dimensional variables and the nondimensional quantities are given for some typical mesometeorological vortices. For convenience only the quantities associated with the simple cases of angular momentum with n = 1.0 and n = 0.5 are shown. This table shows that vertical velocity at the top of the surface layer, w_s, corresponding to a value of pumping of h_o = 0.2 may range from 0.6 cm s^{-1} to 12.6 cm s^{-1} for commonly occurring meso vortices, which is quite reasonable.

As more and more data on meso vortices become available through double doppler radar,or other means optimism exists for the development of more sophisticated theoretical models of these vortices in the near future.

ACKNOWLEDGMENTS

The authors received valuable advice from Professor A. Garder of the Southern Illinois University and Professor Y. J. Lin of Saint Louis University during the course of the investigation. The research was sponsored by Grant No. 04-6-022-44003 of the National Severe Storms Laboratory (NOAA, U. S. Dept. of Commerce) and ATM74-09448-A02 of the National Science Foundation.

APPENDIX A

DETAILS OF THE NUMERICAL METHODS

An effective numerical method for solving nonlinear boundary value problems of the type Eqs. 2.4 and 2.5 is the Newton's iterative method (Keller, 1968 and Collatz, 1968). This technique along with the Gaussian integration to solve Eq. 2.6 is described in the following.

Subdivide the interval $(0, \delta_\eta)$ into units of constant length $h = \eta_{i+1} - \eta_i$ by the partition

$$0 = \eta_0 < \eta_1 < \cdots < \eta_{n+1} = \delta_\eta$$

Now discretize Eqs. 2.4 and 2.5 using centered differences. We denote the resulting nonlinear difference equivalent vectorially by

$$\tilde{\Phi} = 0 \qquad \text{(A1)}$$

where the i^{th} component is $\Phi_i = (\Psi_{1i}, \Psi_{2i})^T$, $(i = 1, \cdots M)$, and

$$\Psi_{1i} \equiv \left[1 - \frac{(n+1)h}{2} H_i\right] F_{i+1} - \left[2 + (1-2n)h^2 F_i\right] F_i + \left[1 + \frac{(n+1)h}{2} H_i\right] F_{i-1} - h^2 G_i^2 + h^2 = 0,$$

$$\Psi_{2i} \equiv \left[1 - \frac{(n+1)h}{2} H_i\right] G_{i+1} + \left[-2 + 2n h^2 F_i\right] G_i + \left[1 + \frac{(n+1)h}{2} H_i\right] G_{i-1} = 0.$$

The superscript T denotes the transpose, h the step size and $F_i = F(\eta_i)$, $G_i = G(\eta_i)$ and $H_i = H(\eta_i)$. For any initial estimate of $s_i = (F_i, G_i)^T$, $(i = 1, \ldots, M)$, define an iterative process

$$\tilde{S}^{(k+1)} = \tilde{S}^{(k)} - \Delta\tilde{S}^{(k)}, \quad k = 0, 1, \cdots,$$

where $\Delta \tilde{s}^{(k)}$ is the correction applied to the most recent, k^{th}, iterative estimate. $\Delta \tilde{s}^{(k)}$ is the solution of

$$D \Delta \tilde{s}^{(k)} = \tilde{\phi}^{(k)}, \quad k = 0, 1, \ldots . \tag{A2}$$

D is a block tridiagonal matrix representing the Jacobian of $\tilde{\phi}$ evaluated using the k^{th} iterative estimates and has the form,

$$D = \begin{pmatrix} B_1 & C_1 & & & \\ A_2 & B_2 & C_2 & & \\ & \ddots & \ddots & \ddots & \\ & & A_{M-1} & B_{M-1} & C_{M-1} \\ & & & A_M & B_M \end{pmatrix},$$

where in general

$$A_i = \begin{pmatrix} \frac{\partial \Psi_{1i}}{\partial F_{i-1}} & \frac{\partial \Psi_{1i}}{\partial G_{i-1}} \\ \frac{\partial \Psi_{2i}}{\partial F_{i-1}} & \frac{\partial \Psi_{2i}}{\partial G_{i-1}} \end{pmatrix},$$

$$B_i = \begin{pmatrix} \frac{\partial \Psi_{1i}}{\partial F_i} & \frac{\partial \Psi_{1i}}{\partial G_i} \\ \frac{\partial \Psi_{2i}}{\partial F_i} & \frac{\partial \Psi_{2i}}{\partial G_i} \end{pmatrix},$$

$$C_i = \begin{pmatrix} \frac{\partial \Psi_{1i}}{\partial F_{i+1}} & \frac{\partial \Psi_{1i}}{\partial G_{i+1}} \\ \frac{\partial \Psi_{2i}}{\partial F_{i+1}} & \frac{\partial \Psi_{2i}}{\partial G_{i+1}} \end{pmatrix} \text{ and}$$

$\Delta \tilde{s}$ is found by using (block tridiagonal) Gaussian elimination (Varga, 1962).

With each iteration improved estimates for F_i and G_i, (i=1,...,M), are obtained. Using a Gaussian-type integration, (see Conte and deBoor, 1972) Eq. 2.6 is solved for H_i, (i=1,... M+1), using the latest estimates of the F_i's. This cycle is then repeated till a desired accuracy is achieved.

One interesting point in this process is the way in which the upper boundary conditions, i.e., at δ_η, are handled. Since the position of δ_η is not really known an educated guess must be made. If the residual, i.e., a numerical approximation to equation (A1) is small on the estimated interval $(0, \delta_\eta)$ and the boundary conditions are also satisfied then δ_η is accepted as the top of the boundary layer. Otherwise δ_η is increased thus changing the order of matrix D. If in the adjustment process the desired programming limitations are exceeded as based on step size, storage or computing time then the upper boundary conditions must be reformulated. In the latter case we obtain the solutions over a desired range by using the approach suggested by Froese (1962). This method replaces the boundary conditions in question with $F_{M+1} = c_1 F_M$ and $G_{M+1} = c_2 G_M$, where the constants c_1 and c_2 are determined from asymptotic expansions or from physical insight. In our case we choose $c_1 = c_2 = 1.0$. All interpolations performed in the integration process are made using a cardinal cubic spline (Nilson, 1970). The numerical procedure for handling the lower boundary conditions are the same used by Kuo (1971).

In most of the experiments the interval $[0, \delta_\eta]$ was divided into 200 equal parts with h = 0.1* while in some into 450 with the same h. Convergence was attained when the largest absolute difference between two successive iterated dimensionless motion field components, e.g., V is less than 10^{-5} in the entire domain.

---

* Tests of various step sizes show that h = 0.1 gives satisfactory accuracy.

APPENDIX B

TABULAR VALUES OF SOME DIMENSIONAL AND NONDIMENSIONAL QUANTITIES ASSOCIATED WITH MESOMETEOROLOGICAL VORTICES

TABLE 2. δ_R: Reference boundary depth (m); V_m: maximum tangential velocity (m s^{-1}); r_m: radius (m) of maximum tangential velocity; $\bar{\nu}$: eddy viscosity (m^2 s^{-1}) coefficient; w_s: vertical velocity (m s^{-1}) at the top of the sublayer corresponding to the nondimensional $h_o = 0.2$; $\bar{K}$:$K\bar{z}\eta^{-1}$ where $\bar{z}$ is the dimensional height (m) and η is its nondimensional counterpart; n: the coefficient in the power law; r: dimensionless radius; K: nondimensional Taylor coefficient ($=F/dF/d\eta$); $\bar{u} = -V_m F$; and $\bar{v} = V_m G$.

	Non-dimensional Quantities		
	n = 1 r = 1 K = 1	n = .5 r = 2 K = 1	n = .5 r = 5 K = 1
Dimensional Quantities			
δ_R = 500 V_m = 10 r_m = 1000 $\bar{\nu}$ = 10	w_s = .126 K = 31.600	w_s = .067 K = 44.68	w_s = .009 K = 70.660

REFERENCES

Bode, L., L. M. Leslie, and R. K. Smith, 1975: A numerical study of boundary effects on concentrated vortices with application to tornadoes and watersprouts. Q. J. Roy Met. Soc., 101, 313-324.

Boedewadt, von U. T., 1940: Die Drehströmung über festem Grunde. Z. angew Math. Mech., 20, 241-253.

Brandes, E. A., 1977: Flow in severe thunderstorms observed by dual-doppler radar. Mon. Wea. Rev., 105, 113-120.

Burggraf, O., K. Stewartson, and R. Belcher, 1971: Boundary layer induced by a potential vortex. Phys. Fluids, 14, 1821-1833.

Burggraf, O. R., and K. Stewartson, 1975: The ladder structure of the generalized vortex. Z. angew. Math. Phys., 26, 549-559.

Chi, S. W., 1974: Numerical modeling of the three-dimensional flows in the ground boundary layer of a maintained axi-symmetrical vortex. Tellus, 4, 444-455.

Collatz, L., 1966: Functional Analysis and Numerical Mathematics. Academic Press, 473 pp.

Conte, S. D., and C. deBoor, 1972: Elementary Numerical Analysis: An Algorithmic Approach. McGraw-Hill, 396 pp.

Davies-Jones, R. P., and G. T. Vickers, 1971: Numerical simulation of convective vortices, NOAA Tech. Memo. ERL-NSSL 1957, Norman, Okla., 27 pp.

Debnath, L., and S. Mukherjee, 1973: Unsteady multiple boundary layers on a porous plate in a rotating system. Phys. Fluids, 16, 1418-1421.

Eliassen, A., 1971: On the Ekman layer in a circular vortex. J. Met. Soc. Jap., 49, 209-214.

Evans, D. J., 1969: The rotationally symmetric flow of a viscous fluid in the presence of an infinite rotating disc with uniform suction. Q. J. Mech. Appl. Math., 22, 467-485.

Froese, C., 1962: On solving $y''=fy+g$ with a boundary condition at infinity. Math. Comp., 16, 492-494.

Fujita, T. T., and F. Caracena, 1977: An analysis of three weather-related aircraft accidents. To appear shortly in Bull. Amer. Met. Society, 1977. Mentioned in that article is a reference to an earlier study by T. T. Fujita bearing the title, "Overshooting thunderheads observed from ATS and Lear jet". SMRP Research Paper number 117 of Univ. of Chicago, 1974, pp. 29.

Keller, H. B., 1968: Numerical Methods for Two Point Boundary Value Problems. Blaisdell Publishing Co., 184 pp.

King, W. S., and W. S. Lewellen, 1964: Boundary-layer similarity solutions for rotating flows with and without magnetic interaction. Phys. Fluids, 7, 1674-1680.

Kuiken, H. K., 1971: The effect of normal blowing on the flow near a rotating disk of infinite extent. J. Fluid Mech., 47, 789-798.

Kuo, H. L., 1971: Axisymmetric flow in the boundary layer of a maintained vortex. J. Atmos. Sci., 28, 20-41.

Mack, L. M., 1962: The laminar boundary layer on a disk of finite radius in a rotating flow. Jet Propulsion Lab., Tech. Rept. 32-224, California Institute of Technology, 46 pp.

Nguyen, N. D., J. P. Ribault, and P. Florent, 1975: Multiple solutions for flow between coaxial disks. J. Fluid Mech. 68, 369-388.

Nilson, F. N., 1970: Cubic splines on uniform meshes. Com. of the ACM, 13, 255-258.

Ray, P. S., 1976: Vorticity and divergence fields within tornadic storms from dual doppler observations. J. Appd. Meteor., 15, 879-890.

Rogers, M. H., and G. N. Lance, 1960: The rotationally symmetric flow of a viscous fluid in the presence of an infinite disk. J. Fluid Mech., 7, 617-631.

_____, 1964: The boundary layer on a disc of finite radius in a rotating fluid. Q. J. Mech. Appl. Math., 17, 319-330.

Rott, N., and W. S. Lewellen, 1964: Boundary layers in rotating flows. Proc. Eleventh Intern. Congress Applied Mechanics, Berlin, Springer-Verlag, 1030-1036.

Schlichting, H., 1968: Boundary Layer Theory, McGraw-Hill, 748 pp.

Serrin, J., 1972: The swirling vortex. Phil. Trans., 271, 325-360.

Sparrow, F. M., and J. L. Gregg, 1960: Mass transfer, flow and heat transfer about a rotating disk. J. Heat Transf., 82, 294-302.

Stuart, J. T., 1954: On the effect of uniform suction on the steady flow due to a rotating disk. Q. J. Mech. Appl. Math., 7, 446-457.

Taylor, G. I., 1915: Eddy motion in the atmosphere. Phil. Trans. Roy. Soc. London, A215, 1-26.

Varga, R. S., 1962: Matrix Iterative Analysis, Prentice-Hall, 322 pp.

Watson, E. J., 1966: The equation of similar profiles in boundary layer theory with strong blowing. Proc. Roy. Soc., A294, 208-234.

Wylie, C. R., Jr., 1966: Advanced Engineering Mathematics, McGraw-Hill, 813 pp.

List of Figures

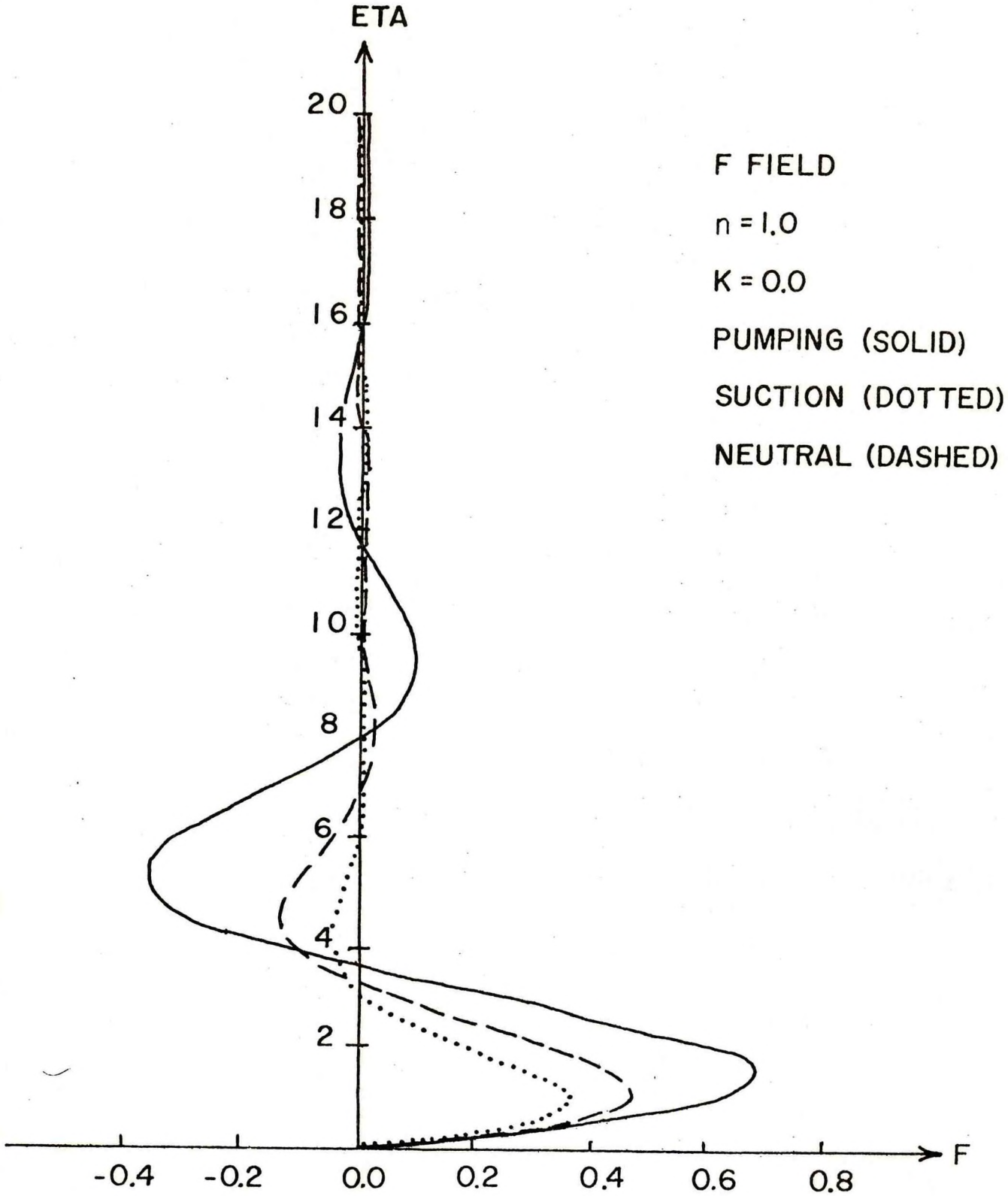
ETA
20
18
16
14
12
10
8
6
4
2
-0.4
-0.2
0.0
0.2
0.4
0.6
0.8
F
F FIELD
n = 1.0
K = 0.0
PUMPING (SOLID)
SUCTION (DOTTED)
NEUTRAL (DASHED)

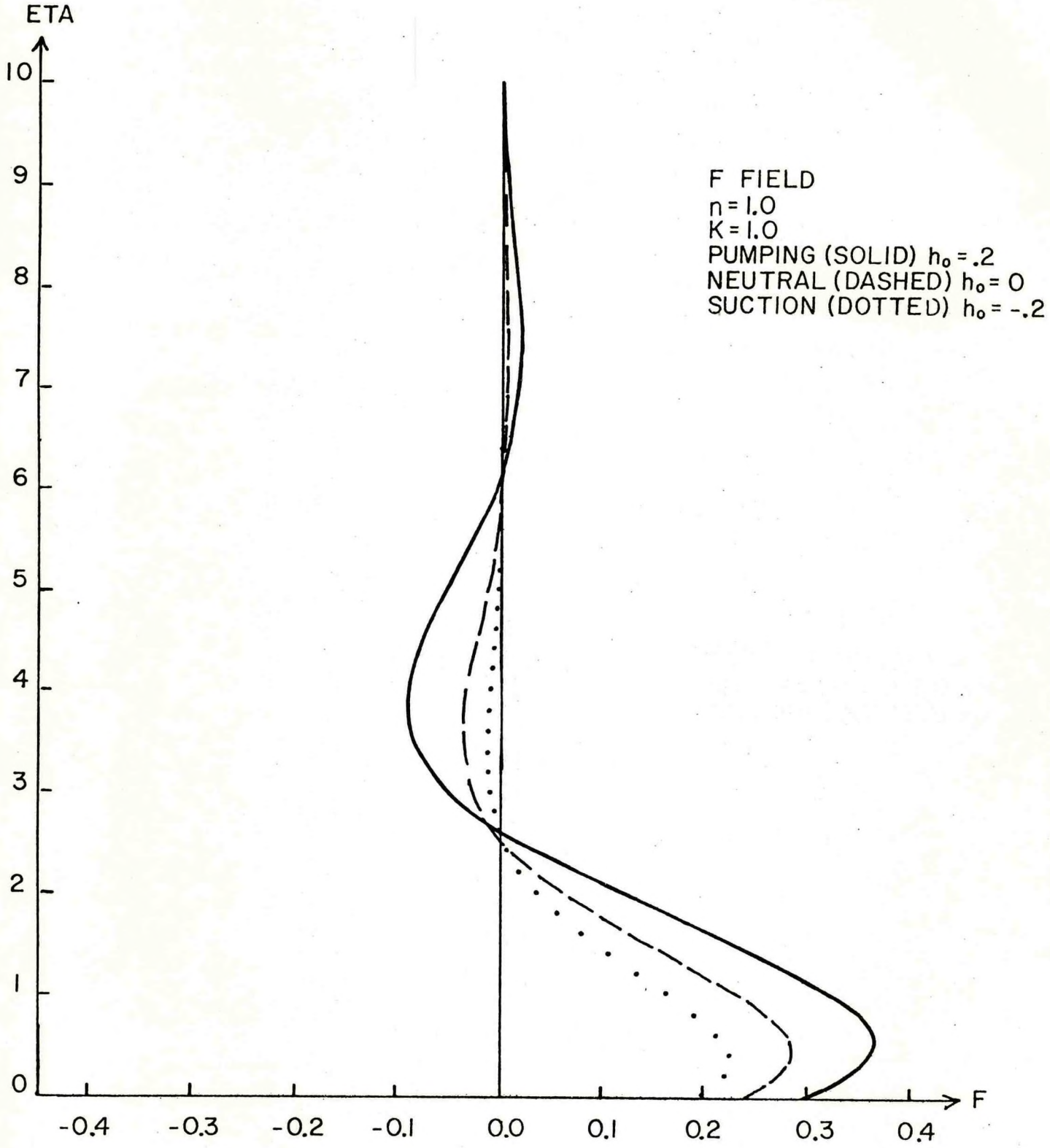
ETA
10
9
8
7
6
5
4
3
2
1
0
F FIELD
n = 1.0
K = 1.0
PUMPING (SOLID) h_o = .2
NEUTRAL (DASHED) h_o = 0
SUCTION (DOTTED) h_o = -.2
-0.4
-0.3
-0.2
-0.1
0.0
0.1
0.2
0.3
0.4
F

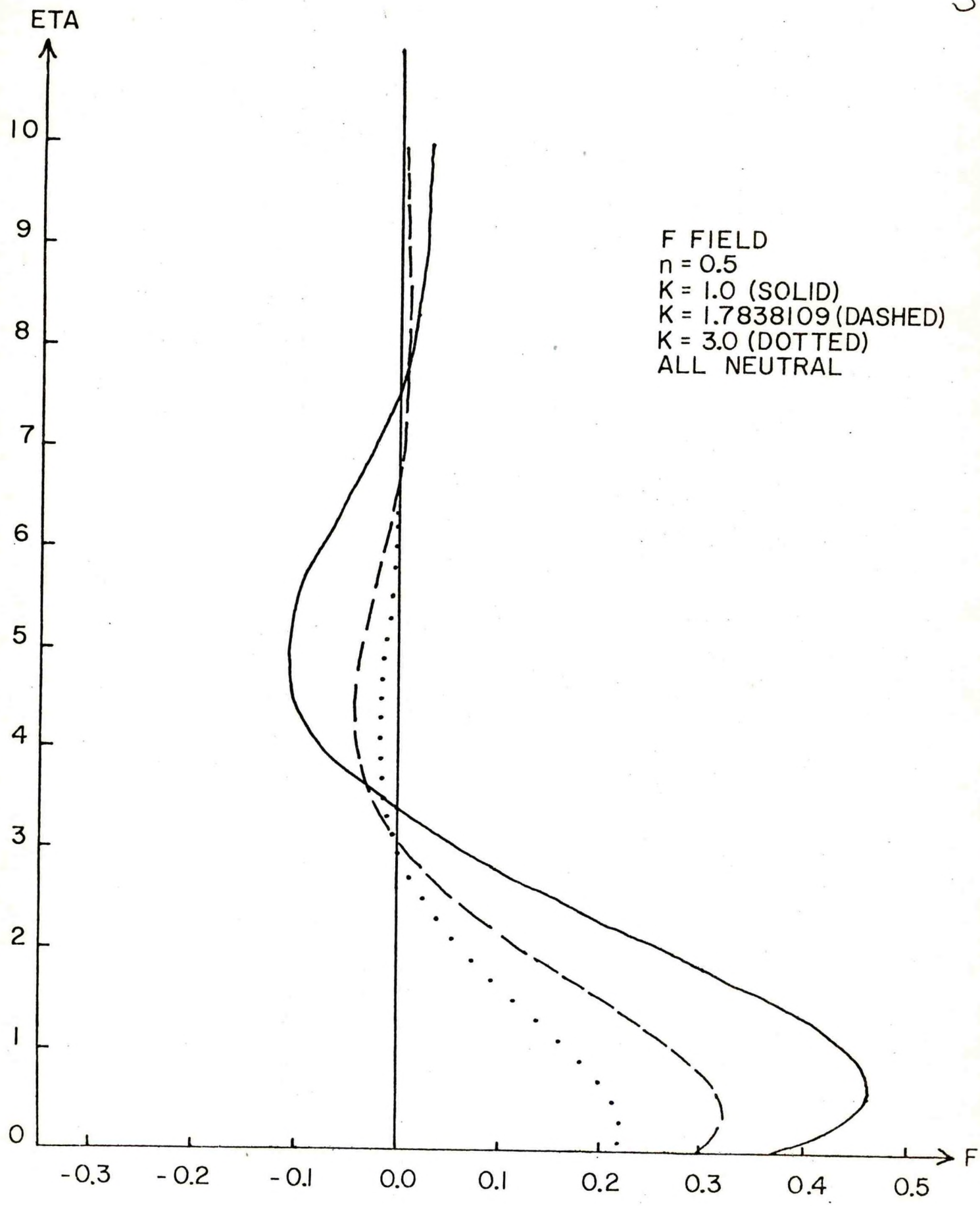
ETA
10
9
8
7
6
5
4
3
2
1
0
-0.3
-0.2
-0.1
0.0
0.1
0.2
0.3
0.4
0.5
F
F FIELD
n = 0.5
K = 1.0 (SOLID)
K = 1.7838109 (DASHED)
K = 3.0 (DOTTED)
ALL NEUTRAL

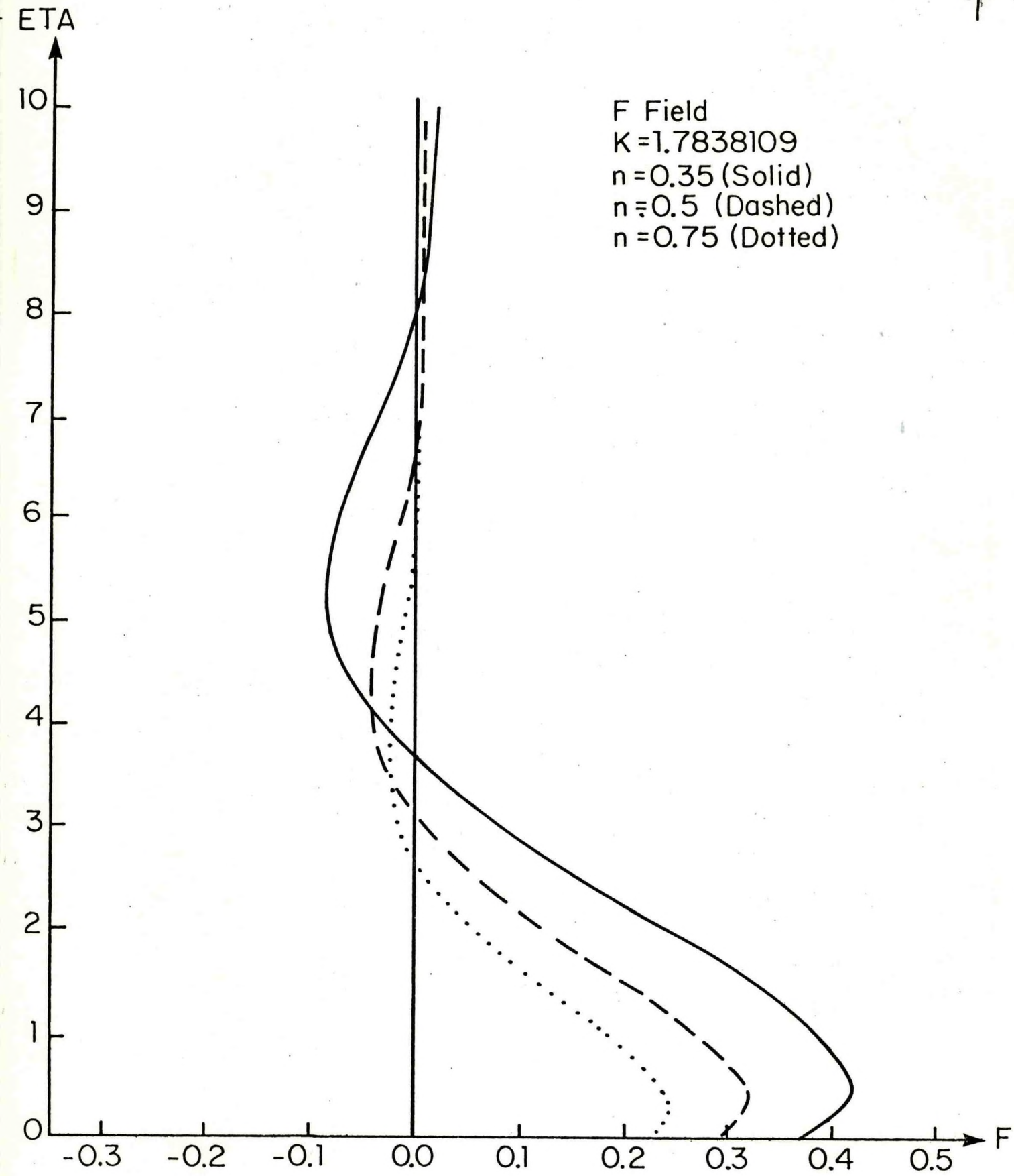
ETA
10
9
8
7
6
5
4
3
2
1
0
F Field
K=1.7838109
n=0.35 (Solid)
n=0.5 (Dashed)
n=0.75 (Dotted)
-0.3
-0.2
-0.1
0.0
0.1
0.2
0.3
0.4
0.5
F

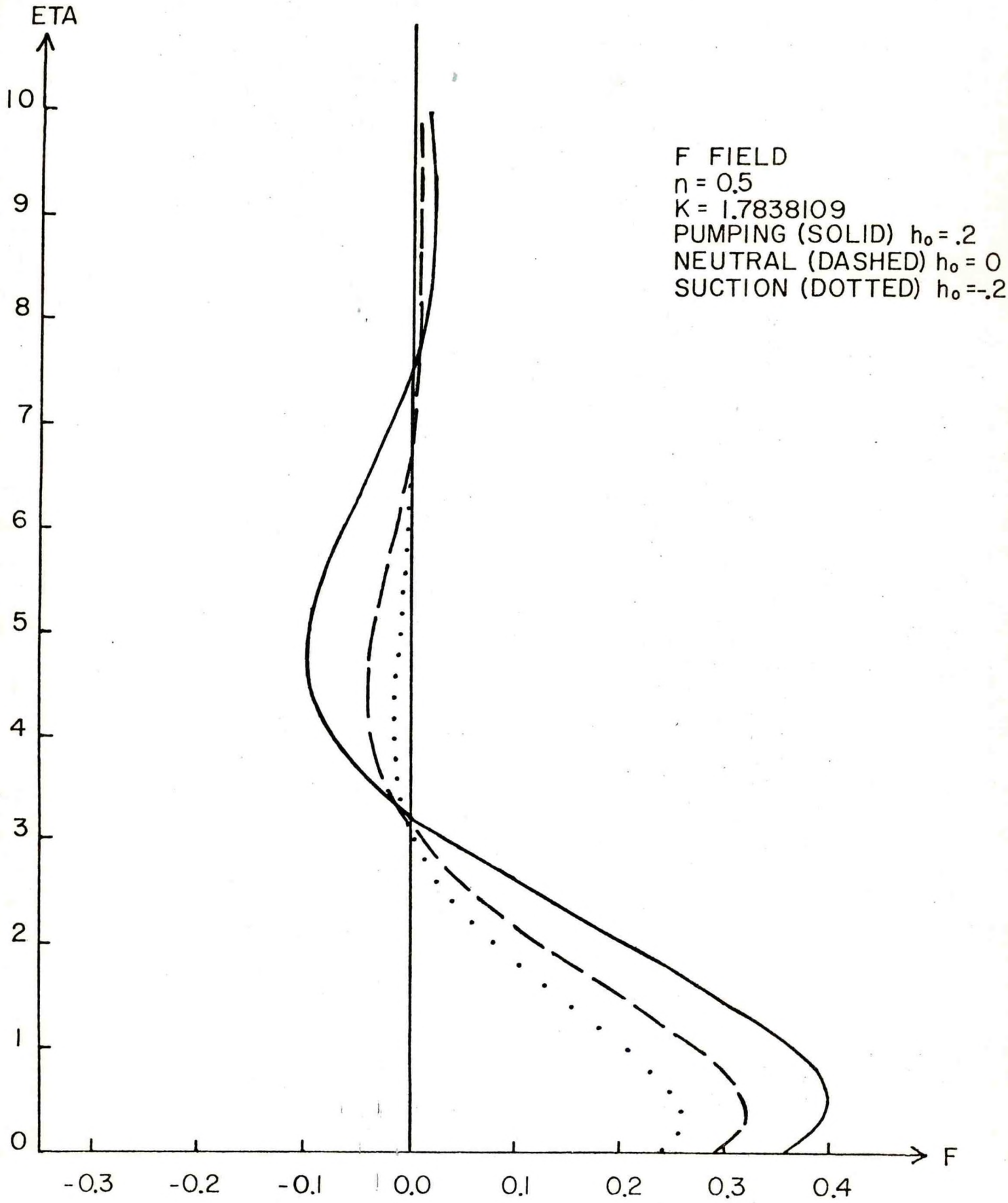
ETA
10
9
8
7
6
5
4
3
2
1
0
-0.3
-0.2
-0.1
0.0
0.1
0.2
0.3
0.4
F
F FIELD
n = 0.5
K = 1.7838109
PUMPING (SOLID) h_o = .2
NEUTRAL (DASHED) h_o = 0
SUCTION (DOTTED) h_o =-.2

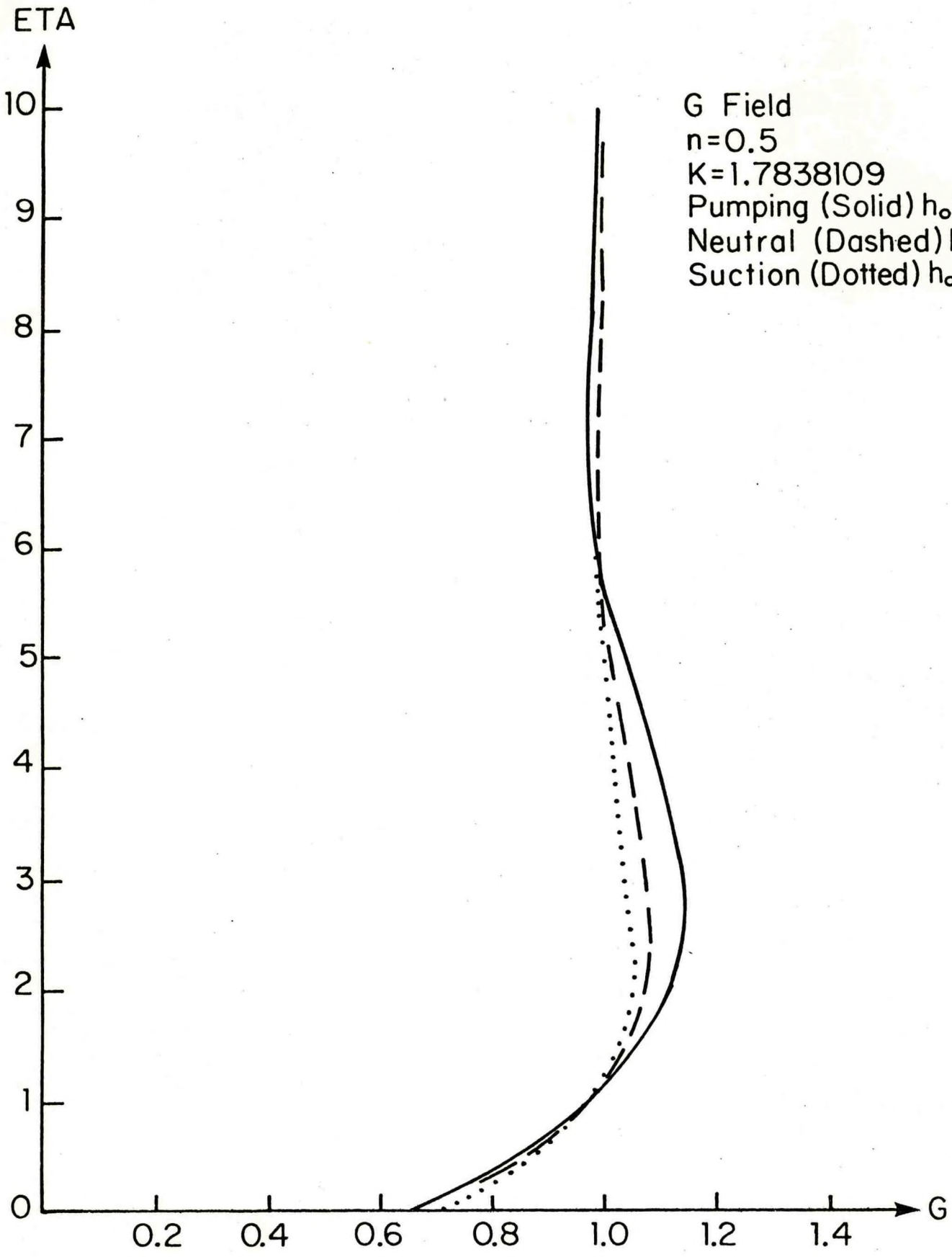
ETA
10
9
8
7
6
5
4
3
2
1
0
0.2
0.4
0.6
0.8
1.0
1.2
1.4
G
G Field
n=0.5
K=1.7838109
Pumping (Solid) h_o=.2
Neutral (Dashed) h_o=0
Suction (Dotted) h_o=.2

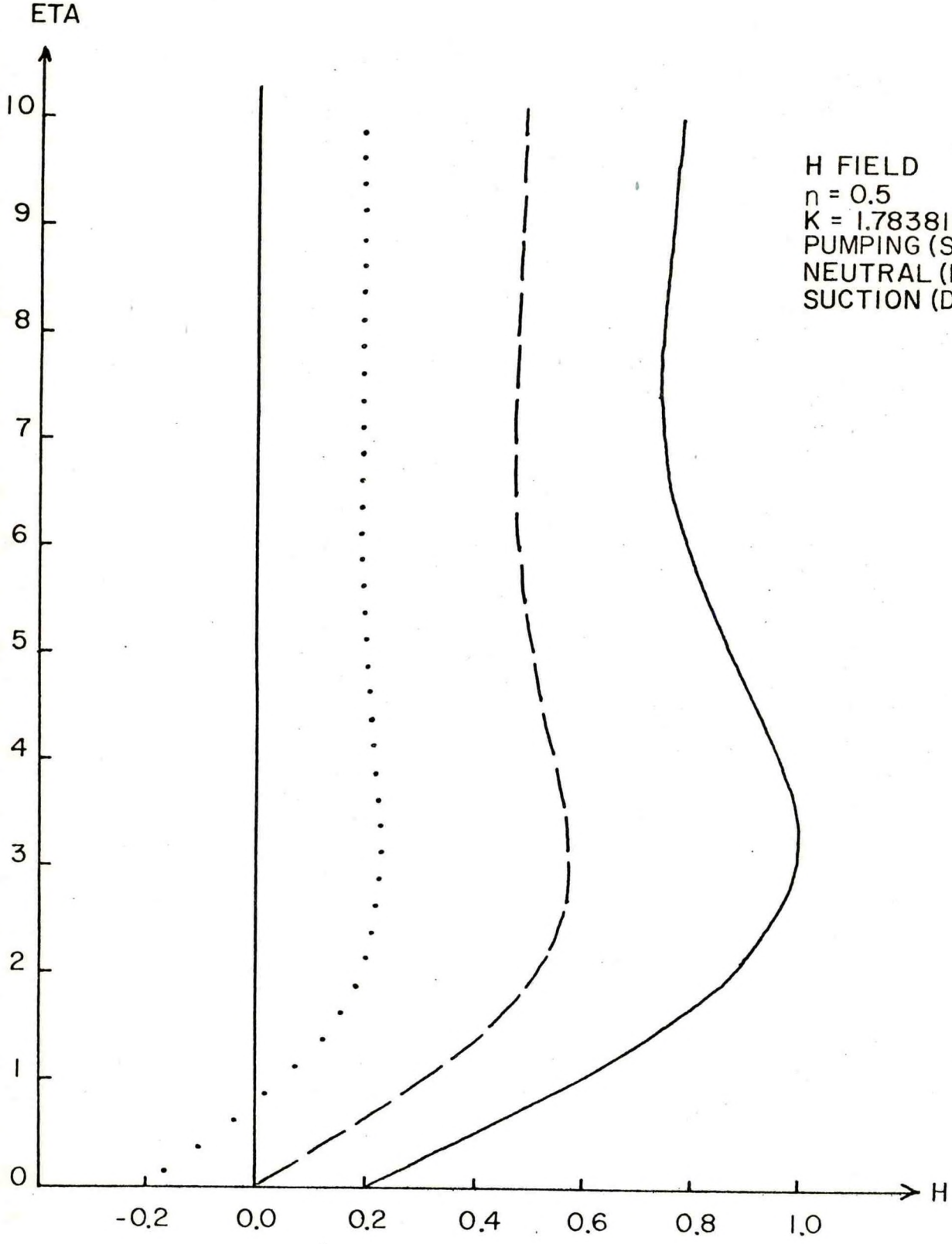
ETA
10
9
8
7
6
5
4
3
2
1
0
-0.2
0.0
0.2
0.4
0.6
0.8
1.0
H
H FIELD
n = 0.5
K = 1.7838109
PUMPING (SOLID) h_o = .2
NEUTRAL (DASHED) h_o = 0
SUCTION (DOTTED) h_o = -.2

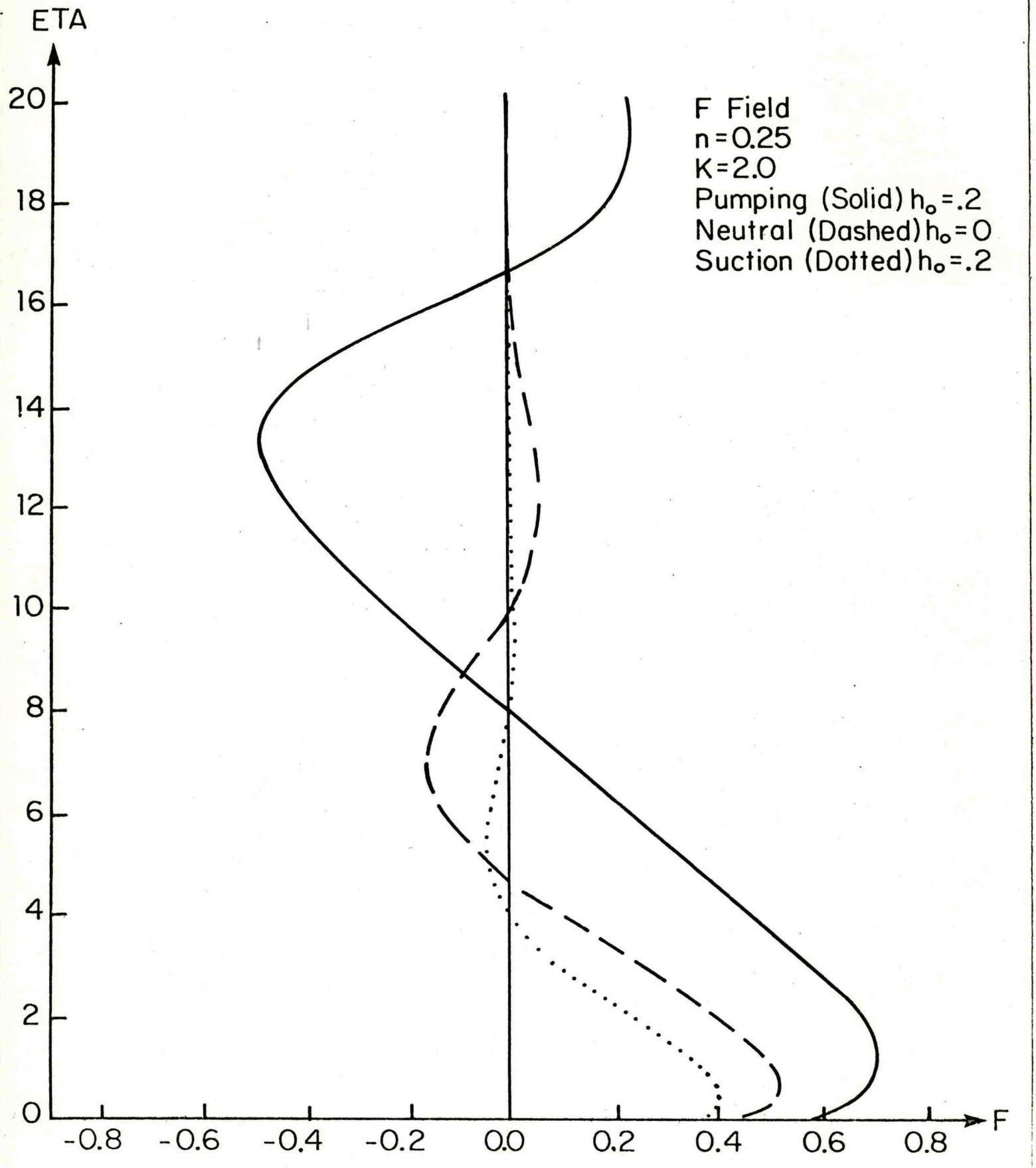
ETA
20
18
16
14
12
10
8
6
4
2
0
-0.8
-0.6
-0.4
-0.2
0.0
0.2
0.4
0.6
0.8
F
F Field
n=0.25
K=2.0
Pumping (Solid) h_o=.2
Neutral (Dashed) h_o=0
Suction (Dotted) h_o=.2

PART II: BOUNDARY LAYER DYNAMICS OF A DECAYING VORTEX CORE

by

William H. Raymond and G. V. Rao
Dept. of Earth and Atmospheric Sciences
Saint Louis University

ABSTRACT

The rapid transient motions within a decaying axisymmetric vortex boundary layer are analyzed for various 'local' Rossby and Reynolds numbers. Both laminar (no-slip) and turbulent (slip) boundary conditions are considered for flows over rotating and stationary surfaces. Similarity transformations are performed by expanding the velocity components in powers of a ratio of dimensionless radius to time. The zeroth-order system described by two nonlinear second order ordinary differential equations is solved by Newton's iterative method. Comparisons are made with Hatton (1975) for the special case of laminar flow over a stationary surface. For the first-order system, asymptotic solutions representing the flow far above the lower surface are obtained.

For laminar flow our results indicate that the vertical velocity is either only downward, both upward and downward (thus an axial stagnation point exists) or only upward motion depending on the value of the Rossby (Reynolds) number. Turbulent conditions are shown to produce only negative (downward) vertical velocities. The presence of an axial stagnation point and the value of the Reynolds number for which the axial motion (laminar, zeroth-order) becomes completely downward corresponds with the findings of Hatton (1975). The addition of mass as simulated by blowing is shown to effectively delay the decay process.

1. Introduction

The boundary layers of concentrated vortices in the atmosphere, e.g., a tornado, have been simulated by many laboratory and theoretical investigations (for a comprehensive review see Davies-Jones and Kessler, 1974). Even studies of the steady-state problem have encountered difficulties. They are primarily due to the fact that the tangential velocity profile near the top of the boundary layer changes radically with the radial distance, the governing partial differential equations are nonlinear, and the lower boundary conditions are hard to satisfy. Additional problems confronted the theoretical study of decaying vortices (Oseen, 1911; Rott, 1958, 1959; Bellamy-Knights, 1970, 1971, 1974; Hatton, 1975). For example, a knowledge of the initial velocity profiles is demanded. These are poorly known at present. Also the relationship at the top of the boundary layer between the tangential velocity component and the radial pressure gradient and the nature of their time dependence have not been clearly documented.

The boundary layer dynamics within the inner portion of a rapidly decaying vortex is of interest in this study. The decay is characterized by the core expanding outward and the radial inflow becoming weakened. The outward expansion itself appears to be more a result of the internal flow dynamics than of diffusion. The rapidity of decay makes observation difficult.

Recent studies by Hatton (1975) of the boundary layer of a decaying vortex inner core showed that for laminar flow and solid rotation the axial motion can be up or down depending upon the value of a parameter proportional to the external angular velocity. Besides, an axial stagnation point was found provided there was radial inflow. The theoretical results were justified by appealing to the observational and laboratory findings (e.g., Rossmann, 1960; Hoecker, 1960; Ward, 1972; Jischke and Parang, 1974; and see also Hsu and Fattahi, 1976).

In the following the governing Navier-Stokes equations are written in dimensionless form and the flow variables are expressed in terms of a power series in r/t, an approach analogous to that suggested by Eliassen (1971). Here r and t are the dimensionless radial and time coordinates. A sufficient condition (not necessary) guaranteeing the validity of this approach is that the ratio r/t is smaller than 1. This places a major restriction on the region of the vortex investigated and the progression of time since the decay process began. This restriction will be clarified later.

The non-dimensionalization process introduces either the 'local' Rossby number R_o or the Reynolds number R_e depending on whether we examine flow over a rotating or rigid surface, respectively. These numbers are defined as

$$R_e = V\delta/\nu \,, \tag{1a}$$

and

$$R_o = V/\delta\Omega_s \,, \tag{1b}$$

where V is the idealized tangential velocity observed at the top of the boundary layer, δ represents a characteristic depth, ν is the kinematic viscosity, and Ω_s is the angular velocity of the rotating solid lower boundary.

In this study the boundary layer dynamics are examined over a wide range of R_o or R_e numbers. Both laminar (no-slip) and turbulent (slip) boundary conditions are considered. For the case of laminar flow the first term approximation predicts an upward vertical motion and an axial stagnation point for a certain range of R_o (R_e). The same approximation for turbulent flow indicates the vertical flow to be downward. However, in both cases it was found that the fluid flow in the boundary layer and in the viscous vortex core far above the boundary are dependent upon the Rossby (Reynolds) number. The nature of these latter motions is predicted from the asymptotic solutions of the similarity equations. These asymptotes indicate that cyclostrophic balance (centrifugal force balancing the horizontal pressure gradient) is quickly attained for Rossby (Reynolds) numbers increasingly larger than one. Suitable similarity transformations are now presented.

2. The mathematical development

Consider an axisymmetric vortex of homogeneous and incompressible fluid with a fixed kinematic viscosity ν.

Let this vortex be in contact with a plane boundary perpendicular to the axis of symmetry. Following a procedure similar to that used by Eliassen (1971) we express dimensional variables, denoted by a bar, in terms of V, Λ_s and δ and introduce the dimensionless variables r, z, t, m, u, w and the transformations

$$\bar{t} = \Lambda_s^{-1} t \quad \text{or} \quad \bar{t} = \delta^2 t \nu^{-1} \tag{2a}$$

depending on whether the flow is over a rotating or fixed lower surface, respectively and

$$\bar{r} = \delta r, \ \bar{z} = \delta z, \ \bar{m} = V m, \ \bar{u} = V u, \ \bar{w} = V w. \tag{2b}$$

Here z denotes the vertical coordinate, r the radial distance from the vortex axis (a quantity that can greatly exceed one) and t the time while m(r,z,t), u(r,z,t) and w(r,z,t) represent the angular, radial and vertical velocity components respectively. In addition, δ on a rotating surface is given by

$$\delta = (\nu/\Lambda_s)^{1/2}.$$

In terms of the dimensionless variables the governing Navier-Stokes equations representing flow over a rotating surface (for flow over a stationary surface replace R_o with R_e) are

$$\frac{\partial}{\partial r}(ru) + r\frac{\partial w}{\partial z} = 0 , \tag{3a}$$

$$\frac{\partial mr^2}{\partial t} + R_o u\frac{\partial mr^2}{\partial r} + R_o w\frac{\partial mr^2}{\partial z} = \frac{\partial^2 mr^2}{\partial z^2} + r\frac{\partial^2 mr}{\partial r^2} + r\frac{\partial m}{\partial r} , \tag{3b}$$

$$\frac{\partial u}{\partial t} + R_o u\frac{\partial u}{\partial r} + R_o w\frac{\partial u}{\partial z} + R_o(\Lambda^2 - m^2)r = \frac{\partial^2 u}{\partial z^2} + \frac{\partial^2 u}{\partial r^2} + \frac{\partial}{\partial r}\left(\frac{u}{r}\right), \tag{3c}$$

for all r, z and $t > 0$. The first is the continuity equation, the second is the equation of motion for the tangential velocity component ($v = mr$) whereas the third relates to the radial component. The nondimensional radial pressure gradient is expressed as $-\Lambda^2 r$ in the last equation. As pointed out by Greenspan (1968) and Barrett (1975) the importance of the nonlinear terms is determined by the R_o or R_e numbers. In the early stages of decay these numbers are fairly large. Alternately, one may define $\tilde{u} = uR_o$, $\tilde{w} = wR_o$, $\tilde{m} = mR_o$ and $\tilde{\Lambda} = \Lambda R_o$ and rewrite equations (3a, b, c). For example the term $R_o(\Lambda^2 - m^2)r$ becomes $(\tilde{\Lambda}^2 - \tilde{m}^2)r$, and the equations do not show the explicit dependence on R_o. But the dependence remains implied through the parameter $\tilde{\Lambda}$, used in describing the radial pressure gradient term.

The lower boundary conditions at $z = 0$ will depend upon whether the flow is laminar or turbulent. With the lower surface in solid rotation ($\bar{m} = \Lambda_s$) the laminar case requires that

$$m = 1/R_o, \quad u = w = 0, \tag{4}$$

at $z = 0$ for all $t > 0$. For the stationary case no-slip boundary conditions require that m is also zero. For the turbulent case the boundary conditions (Taylor, 1916), in dimensionless notation, are:

(on a rotating surface)

$$\frac{\partial m}{\partial z} = C R_o (m - 1/R_o)\left[(m - 1/R_o)^2 r^2 + u^2\right]^{1/2},$$

$$\frac{\partial u}{\partial z} = C R_o u\left[(m - 1/R_o)^2 r^2 + u^2\right]^{1/2}, \tag{5a}$$

(over a stationary surface)

$$\frac{\partial m}{\partial z} = C R_e m\left[m^2r^2 + u^2\right]^{1/2},$$

$$\frac{\partial u}{\partial z} = C R_e u\left[m^2r^2 + u^2\right]^{1/2}, \qquad (5b)$$

and $w = 0$. Here C is the dimensionless drag coefficient.

The exact expressions for the upper boundary conditions are to be determined from asymptotic solutions which are derived from, and are compatible with, the similarity equations. These asymptotes are derived by assuming that for all time $t > 0$ both of the horizontal similarity flow variables become constant sufficiently far above the lower boundary ($z >> 0$). To be physically realistic, above the boundary layer the flow must attain cyclostrophic balance for large Rossby or Reynolds numbers. This may be expressed as

$$m \longrightarrow \Lambda \qquad \text{and} \qquad u \longrightarrow 0$$

as R_o (R_e) becomes large. If the study of a decay of a vortex is contemplated when the initial state is represented by the steady-state the above conditions are also desirable initial conditions at the beginning of the decay process. For Rossby (Reynolds) numbers of order one, transient terms in the equations assume importance so that deviation from the cyclostrophic balance exists.

The z coordinate is now replaced by the similarity variable η where $\eta = z/2t^{1/2}$. In addition, the following expansions, in terms of a power series in r/t, are utilized:

$$m(r,\eta,t) = \frac{1}{t}\left[m_0(\eta) + \frac{r}{t} m_1(\eta) + \cdots \right]$$

$$u(r,\eta,t) = \frac{2^{1/2} r}{t}\left[u_0(\eta) + \frac{r}{t} u_1(\eta) + \cdots \right]$$

$$w(r,\eta,t) = 2\left(\frac{2}{t}\right)^{1/2}\left[w_0(\eta) + \frac{r}{t} w_1(\eta) + \cdots \right] \qquad (6)$$

$$\Omega(r,t) = \frac{1}{t}\left[\Omega_0 + \frac{r}{t}\Omega_1 + \cdots \right] .$$

The initial boundary value problem defined earlier after inserting (6) in equations (3) can now be described by a series of equations in various powers of r/t. This procedure facilitates obtaining mathematical solutions relative easily but their physical interpretation is somewhat complicated.

3. The laminar boundary layer

A. The equations - the zero-order system

Substituting the above expressions into equations (3a, b, c) and collecting terms of the lowest power of r/t gives the zero-order system:

$$2u_0 + w_0' = 0 ,$$

$$-4u_0 - 2\eta u_0' + 2(2)^{1/2} R_0 (2u_0^2 + 2w_0 u_0' + \Omega_0^2 - m_0^2) = u_0'' , \qquad (7)$$

$$-4m_0 - 2\eta m_0' + 4(2)^{1/2} R_0 (2u_0 m_0 + w_0 m_0') = m_0'' .$$

The prime denotes differentiation with respect to η.

B. The upper boundary conditions

Upper boundary conditions are determined by assuming that m_0 and u_0 asymptotically approach constant respective values

for η sufficiently large, i.e., z large or t very small. The asymptotes, as determined from the equations, are

$$m_o = \left(\Lambda_o^2 - \frac{1}{4R_o^2}\right)^{1/2} \quad \text{and} \quad u_o = \frac{1}{2(2)^{1/2}R_o} . \tag{8}$$

We assume that in the limiting process $\bar{v}$ approaches V. This is equivalent to, via (2) and (6), requiring that m_o approach Λ_o. In terms of the original variables the above expressions reduce to upper boundary conditions similar to those used by Hatton (1975). A comparison between Hatton's development of the decay problem and ours is given in Appendix A.

C. The lower boundary conditions

In the case of laminar flow the coupled ordinary differential equations (7) are complemented by lower boundary conditions derived from (4). The zero-order conditions are:

(on a rotating surface)

$$m_o = 1/R_o , \quad u_o = w_o = 0 \qquad \text{at } \eta = 0 ,$$

(on a stationary surface)

$$m_o = u_o = w_o = 0 \qquad \text{at } \eta = 0 .$$

4. Turbulent flow

The zero-order boundary conditions obtained from (5a, b) for the turbulent flow are:

$$m_o' = 0 , \quad u_o' = 0 \qquad \text{and} \quad w_o = 0 \quad \text{when } \eta = 0 . \tag{9}$$

The nonlinear system (7 - 9) has the following solution (which may or may not be unique): $m_o = \left(\Lambda_o^2 - \frac{1}{4R_o^2}\right)^{1/2}$, $u_o = \frac{1}{2(2)^{1/2}R_o}$ and $w_o = -\frac{\eta}{(2)^{1/2}R_o}$.

These expressions are valid provided m_o is well behaved, i.e.,

$$\Lambda_o^2 - \frac{1}{4R_o^2} \geq 0.$$

Note that a degenerate case occurs when $R_o = (2\Lambda_o)^{-1}$., i.e., $m_o = 0$ but u_o and $w_o \neq 0$. The general solution represents a vortex in solid rotation with outward radial and downward vertical motions. The total contribution made by these terms to the boundary layer and viscous vortex depends upon the parameters Λ_o and R_o. It should be noted that the horizontal velocity components near the top of the boundary layer for turbulent flow (zero-order solutions) are identical with the asymptotic zero-order solutions obtained under laminar conditions.

5. Flow near the top of the boundary layer

The asymptotic solutions of the first-order system will be determined for large η. Such solutions will be particularly interesting since they relate to non-solid rotation in the viscous vortex core. Their overall contribution is nevertheless small provided $rt^{-1}\Lambda_1 \ll \Lambda_o$. For large R_o, the restriction on rt^{-1} (given Λ_o, Λ_1, etc) is established by the expression

$$v = \frac{r}{t}\left(\Lambda_o + \frac{r}{t}\Lambda_1 + \cdots\right) = 1$$

because we require that in the limiting process $\bar{v}$ approaches V.

A. The first-order system

Proceeding to the first-order system, obtained by substituting the series (6) into the equations (3a, b, c)

and collecting terms in the next lowest powers of r/t, we obtain

$$3u_1 + w_1' = 0 ,$$

$$-8u_1 - 2\eta u_1' + 4(2)^{1/2} R_0 (3u_0 u_1 + w_0 u_1' + w_1 u_0' + \Lambda_0 \Lambda_1 - m_0 m_1) = u_1'' , \tag{10}$$

$$-8m_1 - 2\eta m_1' + 4(2)^{1/2} R_0 (3u_0 m_1 + w_0 m_1' + w_1 m_0' + 2u_1 m_0) = m_1'' .$$

There is no contribution made by the radial diffusion terms (i.e., radial terms on the right-hand side of equations 3b, c) in the above system since they yield expressions of a different magnitude with respect to r/t.

B. The asymptotic solutions

Assuming that m_1 and u_1 approach constants provided η is sufficiently large, we can compute the asymptotes. They are

$$m_1 = \frac{\Lambda_0 \Lambda_1}{m_0 K} \tag{11}$$

and

$$u_1 = \frac{\Lambda_0 \Lambda_1}{4(2)^{1/2} R_0 m_0^2 K} ,$$

where $$K = 1 + \frac{1}{16 R_0^2 m_0^2} .$$

For R_0 large

$$K \approx 1$$

$$m_1 \approx \Lambda_1$$

and $$u_1 \approx 0.$$

C. Zero and first-order solutions combined

Utilizing (11, 8, 6), we find that at the top of the boundary layer the motion is described by

$$v = \frac{r}{t}\left[m_o + \frac{r}{t}\frac{\Lambda_o \Lambda_1}{m_o K} + \cdots\right],$$
$$u = \frac{r}{t}\left[\frac{1}{2R_o} + \frac{r}{t}\frac{\Lambda_o \Lambda_1}{4R_o m_o^2 K} + \cdots\right], \tag{12}$$

and within this region the vertical velocity behaves as

$$w = -\frac{z}{t}\left[\frac{1}{R_o} + \frac{r}{t}\frac{3\Lambda_o \Lambda_1}{4R_o m_o^2 K} + \cdots\right].$$

Of course the actual or observed vertical velocity at the top of the boundary layer must also include the accumulated effect from the boundary layer. If the above expressions are related back to dimensional variables then we have (for flow over a rotating surface)

$$\bar{v} = R_o \frac{\bar{r}}{\bar{t}}\left[m_o + \frac{R_o \bar{r}}{V\bar{t}}\frac{\Lambda_o \Lambda_1}{m_o K} + \cdots\right],$$
$$\bar{u} = \frac{\bar{r}}{2\bar{t}}\left[1 + \frac{R_o \bar{r}}{V\bar{t}}\frac{\Lambda_o \Lambda_1}{2m_o^2 K} + \cdots\right], \tag{13}$$
$$\bar{w} = -\frac{\bar{z}}{\bar{t}}\left[1 + \frac{R_o \bar{r}}{V\bar{t}}\frac{3\Lambda_o \Lambda_1}{4m_o^2 K} + \cdots\right],$$

where m_o is defined in (8). However, there is a restriction on the ratio $\bar{r}/\bar{t}$. It must satisfy

$$\frac{\bar{r}}{\bar{t}} = \frac{Vr}{R_o t}, \quad \text{or} \quad \frac{\bar{r}}{\bar{t}} = \frac{Vr}{R_e t},$$

depending on which lower boundary conditions are used. The restriction on r/t (Section 5) guarantees that $\bar{v}$ approaches V for R_o (R_e) increasingly large. Similar expressions also describe $\bar{z}/\bar{t}$. Clearly the magnitude of the ratio of V over R_o or V over R_e is established (initially) once Ω_s, δ and ν are assigned values. Note the identities

$$V/R_o = (\nu\Omega_s)^{1/2} \quad \text{and} \quad V/R_e = \nu/\delta .$$

We can now compare equation (13), the solutions at the top of the boundary layer, with the corresponding flow variables used by Hatton (1975): They are

$$\bar{v} = \frac{K_c \bar{r}}{4\pi\bar{t}} , \qquad \bar{u} = \frac{\bar{r}}{2\bar{t}} \tag{14}$$

and

$$w = -\frac{\bar{z}}{\bar{t}} ,$$

where $2\pi K_c$ denotes the circulation. No restrictions were placed on $\bar{r}/\bar{t}$ or $\bar{z}/\bar{t}$, (other comparisons given in Appendix A).

6. A Numerical Method

An effective numerical method for solving the boundary value problem described by equation (7) and the boundary conditions enumerated above is Newton's method (Keller, 1968). This iterative technique permits a very efficient application of the Gaussian elimination procedure. All solutions for the finite difference equivalent of (7) are obtained using a constant step size of $\Delta\eta = .01$. Other details of the computations included the fact that w_o was recalculated during each iteration using a Gaussian integration procedure. The convergence criteria required that the new calculations of u_o

and m_o change by less that 10^{-4}. There was no difficulty in obtaining convergence for all cases tested. The initial guess first used was the steady-state solution due to Boedewadt (1940). The value chosen for Λ_o was one. Interpolation for other values of Λ_o is easily accomplished by using the relationships described in Section 2, i.e., for a specified $\tilde{\Lambda}$ ($\tilde{\Lambda} = R_o \Lambda$), various combinations of R_o and Λ are possible.

The upper boundary conditions are reformulated using an approach suggested by Froese (1962). That is, the boundary conditions are replaced by the expressions

$$u_o^{N+1} = c_1 u_o^N \qquad \text{and} \qquad m_o^{N+1} = c_2 m_o^N$$

implying that between discrete points η_N and η_{N+1} the values of u_o and m_o change by fixed amounts, c_1, and c_2, respectively. The values of c_1 and c_2 can be obtained from the asymptotic solutions. We choose $c_1 = c_2 = 1$ since it is known that for sufficiently large values of η, the independent variable, both m_o and u_o approach a constant.

7. Discussion of laminar results

Figs. 1, 2 and 3, respectively show the numerical solutions for the dimensionless vertical, radial and angular velocity fields (zero-order) for selected Rossby numbers R_o = 1.6, 5.0 and 500. The variation of vertical velocity as a function of R_o is apparent in Fig. 1. For example, the

direction of the axial flow is entirely upward for large R_o's, like 500, and completely downward when R_o is less than or equal to 1.6. When R_o is greater than 1.6 but less than some value, say 10, an axial stagnation point is observed.

Because the variation of R_o influences the solution greatly, we conjecture that no similarity solution of an unsteady vortex for a constant R_o is valid over a broad time period. Even though the entire decay of the vortex core cannot be simulated using a single R_o, several distinct R_o's corresponding to discrete time periods may be employed. Hence η may be thought of as a vertical coordinate since we limit the range or value of t (remembering the restriction on r/t in Section 5). Alternately, z can be held fixed, and variations in η can be interpreted to have been caused by the changes in time. Thus, as Hatton (1975) has indicated, the precise significance of η and how the choices of z, t and r/t should be related to the physical situation is somewhat unclear. A greater observational knowledge of the meteorological vortex should pave the way for an exact choice.

The depth of the boundary layer, the region below that η (interpreting as a vertical coordinate) where u_o and m_o, respectively, reach their asymptotic values given by equation (8), can be easily identified in Figs. 2 and 3. Clearly the boundary layer is depressed when R_o = 500. At this Rossby number a large inflow region exists just above the lower boundary but the dimensionless radial velocity component very

quickly approaches $.707 \times 10^{-3}$ (the asymptotic value) for η larger than .2. When R_o is decreased sufficiently ($R_o < 1.6$) the entire boundary layer is composed of an outward directed radial velocity. Such an outflow is probably responsible for the rapid deterioration in the final or decaying stage of a vortex.

In Fig. 3 we see that the angular velocities' deviation from the cyclostrophic condition that $m_o = \Omega_o$ with $\Omega_o = 1$ at the top of the boundary layer, is small even for $R_o = 1.6$. Significant overshooting of the angular velocity occurs for large Rossby numbers, when the solutions contain oscillations resembling the steady-state profiles which were first given by Boedewadt (1940).

Fig. 4 illustrates how the vertical velocity is affected when the lower boundary condition $w_o = 0$ is replaced with $w_o = h_o$. Physically this is equivalent to replacing the solid rotating lower surface with a perforated boundary through which mass is added by blowing ($h_o > 0$) or mass is removed by suction ($h_o < 0$). The effect of blowing, $h_o = .15$, is to increase the boundary layer thickness and effectively to delay the decay process by intensifying the radial inflow. Just the opposite effect is observed for suction, $h_o = -.15$.

Numerical solutions for flow over a stationary surface, a more geophysically realistic problem, are given in Figs. 5, 6 and 7 for Reynolds numbers $R_e = .755$, 3.0 and 200. The dimensionless vertical velocity, displayed in Fig. 5, is characterized by flow which ranges from completely upward

(R_e = 200) to flow which is entirely downward for R_e less than or equal to .755. A stagnation point exists near the top of the boundary layer when R_e = 3.0.

Figs. 6 and 7 show the dimensionless radial and angular velocities, respectively. These exhibit behavior very similar to those displayed in Figs. 2 and 3, the major differences being the departure from cyclostrophic balance (m_o = 1) at the smaller Reynolds number, and the fact that radial inflow exists for $R_e > .755$ and for $R_o > 1.6$.

8. Conclusions

Our findings show that a stagnation point, as described by Hatton (1975), does occur, during the decay process, within the boundary layer of a vortex core having laminar flow, but only for a limited range of Rossby (Reynolds) numbers. On the other hand, according to the analytical discussion in Section 4, turbulent conditions produce only negative vertical velocities. Ward (1972) postulated that the enlargement observed on a dissipating tornadic funnel represents the transition zone between turbulent flow with negative vertical velocity and the laminar flow, nearest the surface, with its positive vertical motion. Our study gives credence to Ward's speculation on the differences in the direction of the vertical velocity between laminar and turbulent flows. These findings, however, are valid for a relatively short time period typical of the transient decay stage of a vortex.

We have also implied that the outward radial expansion of a vortex or vortex boundary layer during its final stage, once established, is due to the internal dynamics much more than purely diffusionary processes. However, our findings show that this tendency can be slowed or reversed by adding mass as modeled, or simulated, by blowing in this study.

In the final conclusion, we note that the velocity profiles are highly dependent upon the value of R_o (R_e). This is equivalent, in our study, to acknowledging the fact that initial conditions are very important when analyzing non-steady vortices.

ACKNOWLEDGMENTS

This research is sponsored jointly by Grant No. 04-6-022-44003 of the National Severe Storms Laboratory (NOAA, U. S. Dept. of Commerce) and ATM 74-09448-A02 of the National Science Foundation. The principal investigator of the latter grant is Professor Y. J. Lin of Saint Louis University.

APPENDIX A

A Comparison of the Similarity Transformations Used in this Study and Those Due to Hatton (1975)

The first term in our series can be compared with the similarity transformations used by Hatton (1975). Using (1a), (2) and (6) we obtain the following expressions (first term only) for the dimensional velocity components (for flow over a fixed surface)

$$\bar{v} = R_e \frac{\bar{r}}{\bar{t}} m_0(\eta) ,$$

$$\bar{u} = 2^{1/2} R_e \frac{\bar{r}}{\bar{t}} u_0(\eta) , \qquad \text{(A1)}$$

and

$$\bar{w} = 2(2)^{1/2} R_e \left(\frac{\nu}{\bar{t}}\right)^{1/2} w_0(\eta).$$

Hatton used the following similarity transformations: (we have changed his notation slightly for comparison purposes)

$$\bar{v} = \frac{\Omega_H \bar{r}}{4\bar{t}} G(\eta) ,$$

$$\bar{u} = \frac{\bar{r}}{2\bar{t}} F(\eta) , \qquad \text{(A2)}$$

and

$$\bar{w} = -2\left(\frac{\nu}{\bar{t}}\right)^{1/2} H(\eta), \quad \left(\frac{dH}{d\eta} = F\right),$$

where $\eta = z/2t^{\frac{1}{2}}$ or in terms of dimensional variables $\eta = \bar{z}/2\,(\nu \bar{t})^{\frac{1}{2}}$.

This suggests the following relationships:

$$F = 2(2)^{1/2} R_e u_0 , \qquad \text{(A3)}$$

$$G = 4 R_e m_0/\Omega_H , \qquad \text{(A4)}$$

$$H = -(2)^{1/2} R_e w_0 . \qquad \text{(A5)}$$

To obtain the equations used by Hatton it is only necessary to redefine Ω_o^2 by

$$\Omega_o^2 \equiv \frac{\Omega_H^2}{16 R_e^2} + \frac{1}{4R_e^2} , \qquad \text{(A6)}$$

a condition that also follows naturally from (A4) using the asymptotic values of G and m_o, i.e., G = 1 and $m_o = (\Omega_o^2 - 1/4R_e^2)^{1/2}$. These equations may be obtained from (7) using (A3-6), they are:

$$F'' + 2\gamma F' + 4F - 2F^2 + 4HF' + \frac{\Omega_H^2}{2}(G^2 - 1) = 2 , \qquad \text{(A7)}$$

$$G'' + 2\gamma G' + 4G + 4HG' - 4FG = 0 ,$$

and

$$H' - F = 0 .$$

The critical value of Ω_H^2, where the vertical velocity is entirely downward, was found by Hatton to be $\Omega_H^2 = 4.952$. From (A6) we find that

$$R_e^2 = (\Omega_H^2 + 4)/16 , \quad \text{if } \Omega_o = 1 ,$$

and, for $\Omega_H^2 = 4.952$, we obtain the value of $R_e = 0.748$, a quantity reasonably close to our value of $R_e = 0.755$. The slight difference of .007 is probably due to the type of numerical method and to the step size used.

REFERENCES

Barrett, K. E., 1975: Numerical study of the flow between rotating coaxial discs., Z. angew. Math. Phys., 26, 807-817.

Bellamy-Knights, P. G., 1970: An unsteady two-cell vortex solution of the Navier-Stokes equations. J. F. M., 41, 673-687.

_____, 1971: Unsteady multicellular viscous vortices. J. F. M. 50, 1-16.

_____, 1974: An axisymmetric boundary layer solution for an unsteady vortex above a plane. Tellus 3, 318-324.

Boedewadt, von U. T., 1940: Die Drehströmung über festem Grunde. Z. angew Math. Mech., 20, 241-253.

Davies-Jones, R. P., and E. Kessler, 1974: Tornadoes. Weather and Climate Modification, W. N. Hess, Ed., Wiley, 842 pp. (See Chap. 16).

Eliassen, A., 1971: On the Ekman layer in a circular vortex. J. Met. Soc. Japan, 49, 209-214.

Froese, C., 1962: On solving y" = fy - g with a boundary condition at infinity. Math. Comp., 16, 492-494.

Greenspan, H. P., 1968: The Theory of Rotating Fluids. Cambridge University Press, 327 pp.

Hatton, L., 1975: Stagnation point flow in a vortex core. Tellus, 3, 269-279.

Hoecker, W. H., 1960: Wind speed and airflow patterns in the Dallas tornado of 2nd April 1957. M. W. R., 88, 167.

Hsu, C. T., and B. Fattahi, 1976: Mechanism of tornado funnel formation. Physics of Fluids, 19, 1853-1857.

Jischke, M. C., and M. Parang, 1974: Properties of simulated tornado like vortices. J. Atmos. Sci., 31, 506-512.

Keller, H. B., 1968: Numerical Methods for Two Point Boundary Value Problems. Blaisdell Publishing Co., 184 pp.

Oseen, C. W., 1911: Ark f. Math, Astron. och. Fys., 7.

Rossman, F. O., 1960: On the physics of tornadoes. Cumulus Dynamics, p. 167, Pergamon Press, Oxford.

Rott, N., 1958: On the viscous core of a line vortex. Z. angew Math. Phys. 9b, 543-553.

_____, 1959: On the viscous core of a line vortex, II. Z. angew. Math. Phys., 10, 73-81.

Taylor, G. I., 1916: Skin friction of the wind on the earth's surface. Proc. Roy. Soc. A, XCII, 196.

Ward, N. B., 1972: The exploration of certain features of tornado dynamics using a laboratory model. J. Atmos. Sci., 29, 1194-1204.

List of Figures

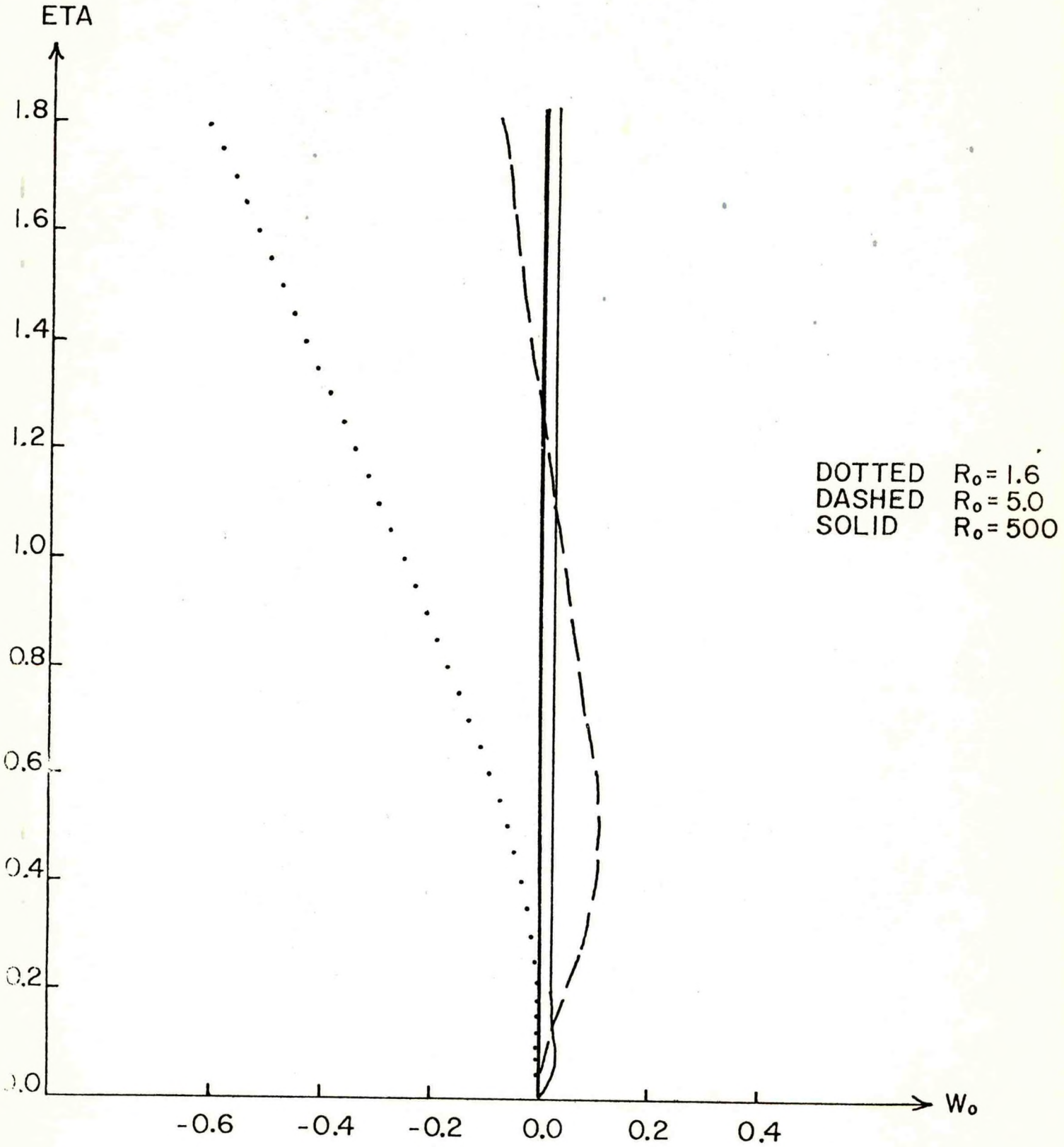
ETA
1.8
1.6
1.4
1.2
1.0
0.8
0.6
0.4
0.2
0.0
-0.6
-0.4
-0.2
0.0
0.2
0.4
W_o
DOTTED $R_o = 1.6$
DASHED $R_o = 5.0$
SOLID $R_o = 500$

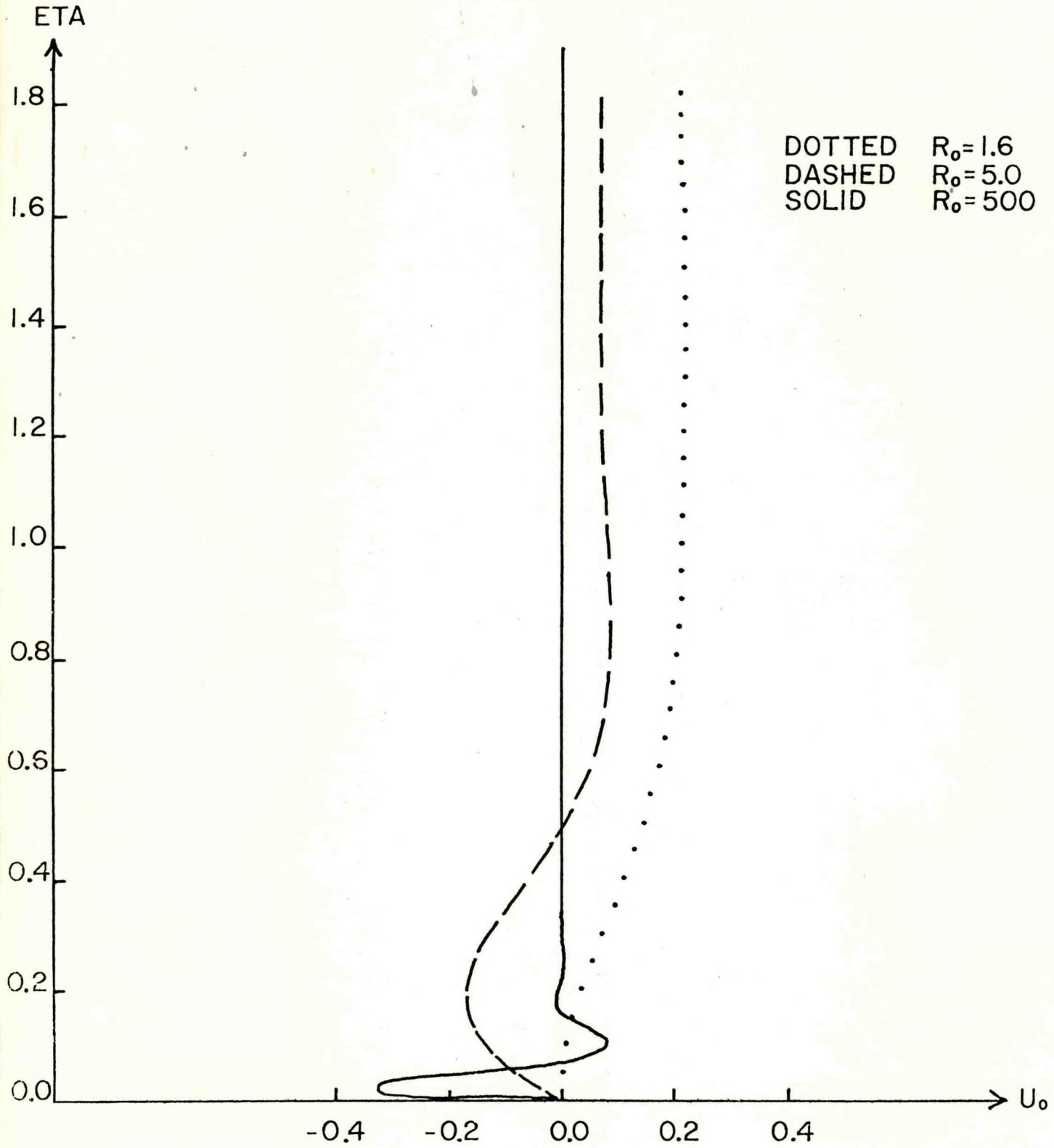
ETA
1.8
1.6
1.4
1.2
1.0
0.8
0.6
0.4
0.2
0.0
DOTTED R_o= 1.6
DASHED R_o= 5.0
SOLID R_o= 500
-0.4
-0.2
0.0
0.2
0.4
U_o

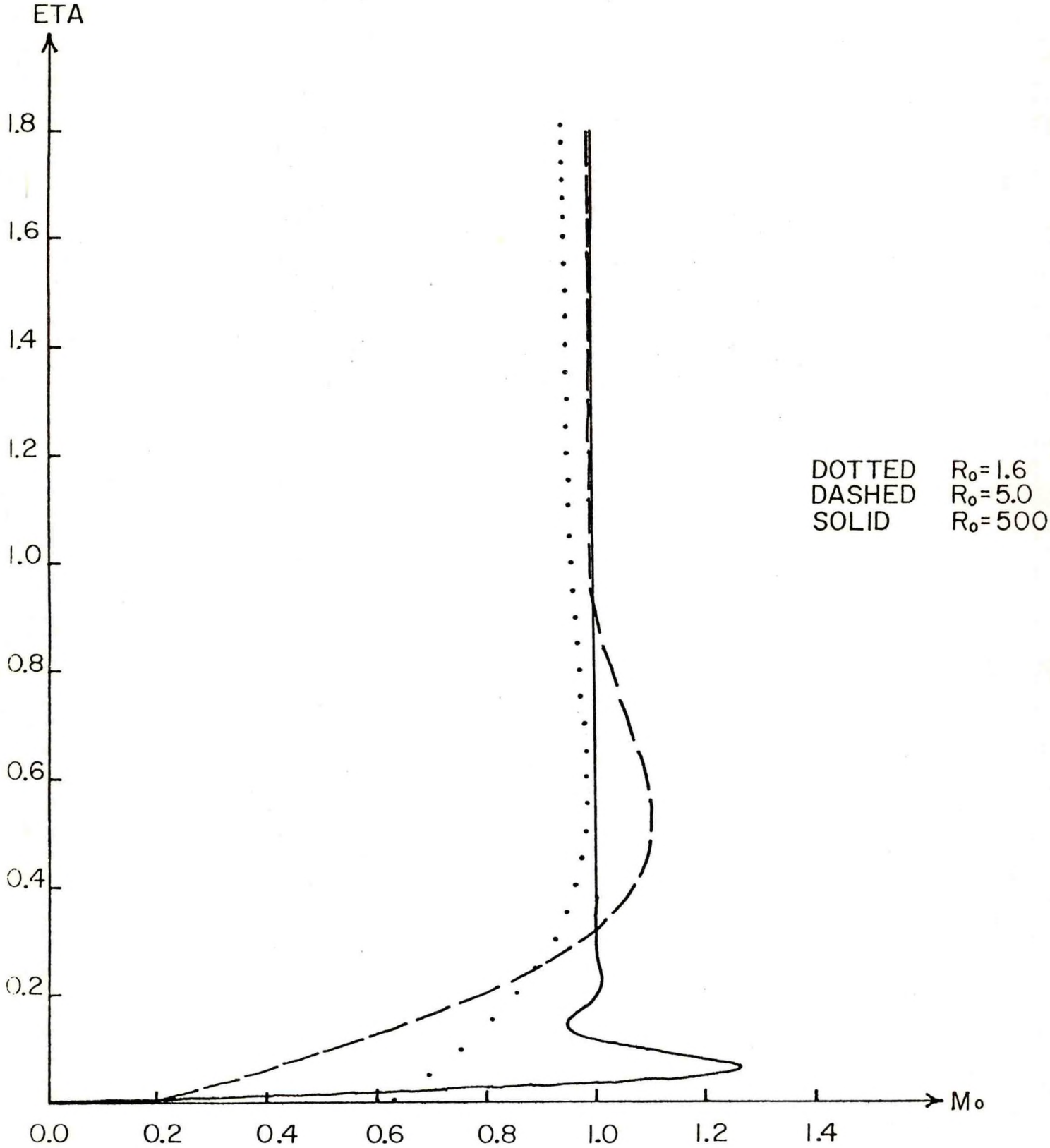
ETA
1.8
1.6
1.4
1.2
1.0
0.8
0.6
0.4
0.2
0.0
0.2
0.4
0.6
0.8
1.0
1.2
1.4
Mo
DOTTED R_o= 1.6
DASHED R_o= 5.0
SOLID R_o= 500

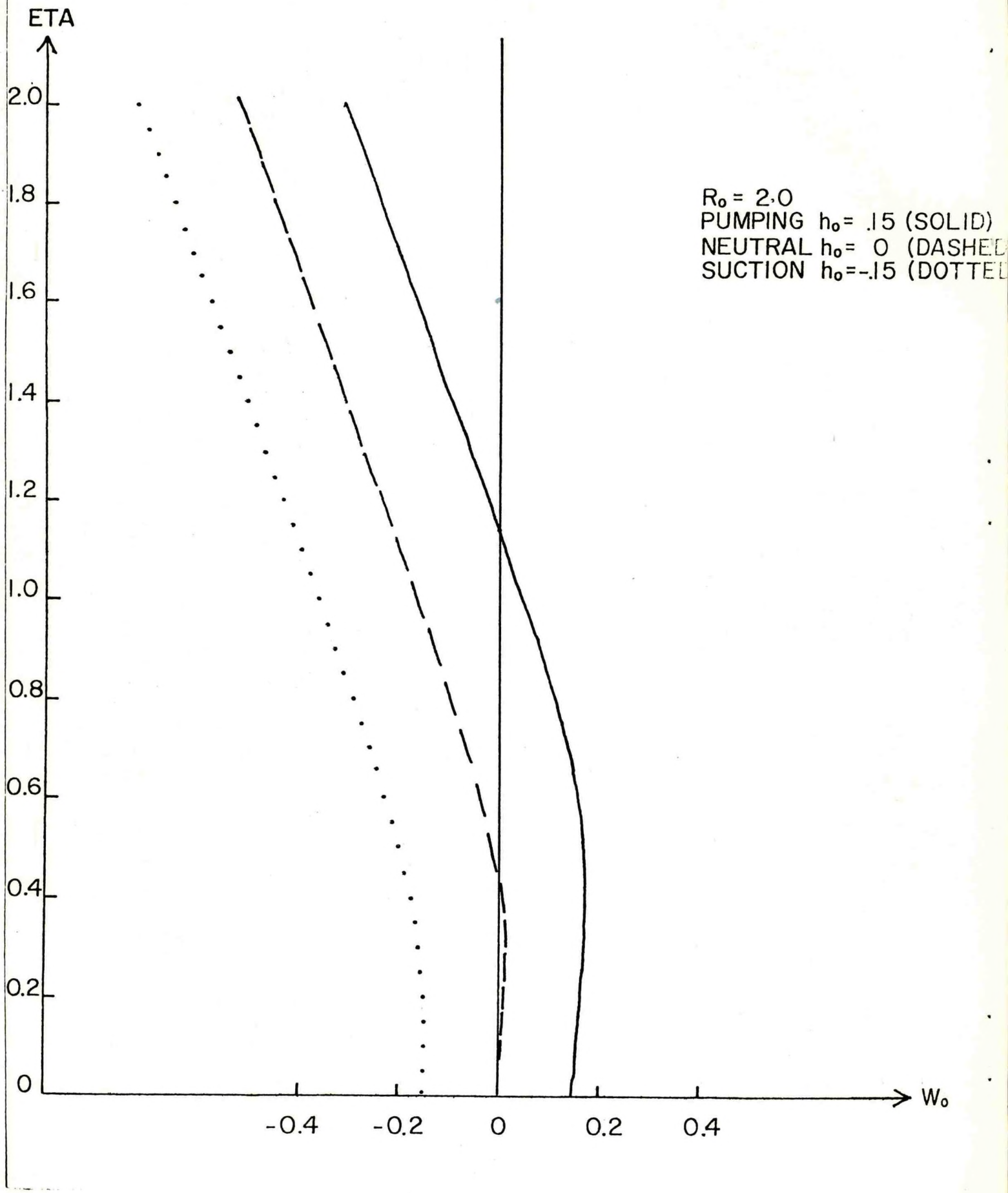
ETA
2.0
1.8
1.6
1.4
1.2
1.0
0.8
0.6
0.4
0.2
0
-0.4
-0.2
0
0.2
0.4
W_o
R_o = 2.0
PUMPING h_o = .15 (SOLID)
NEUTRAL h_o = 0 (DASHED
SUCTION h_o = -.15 (DOTTED

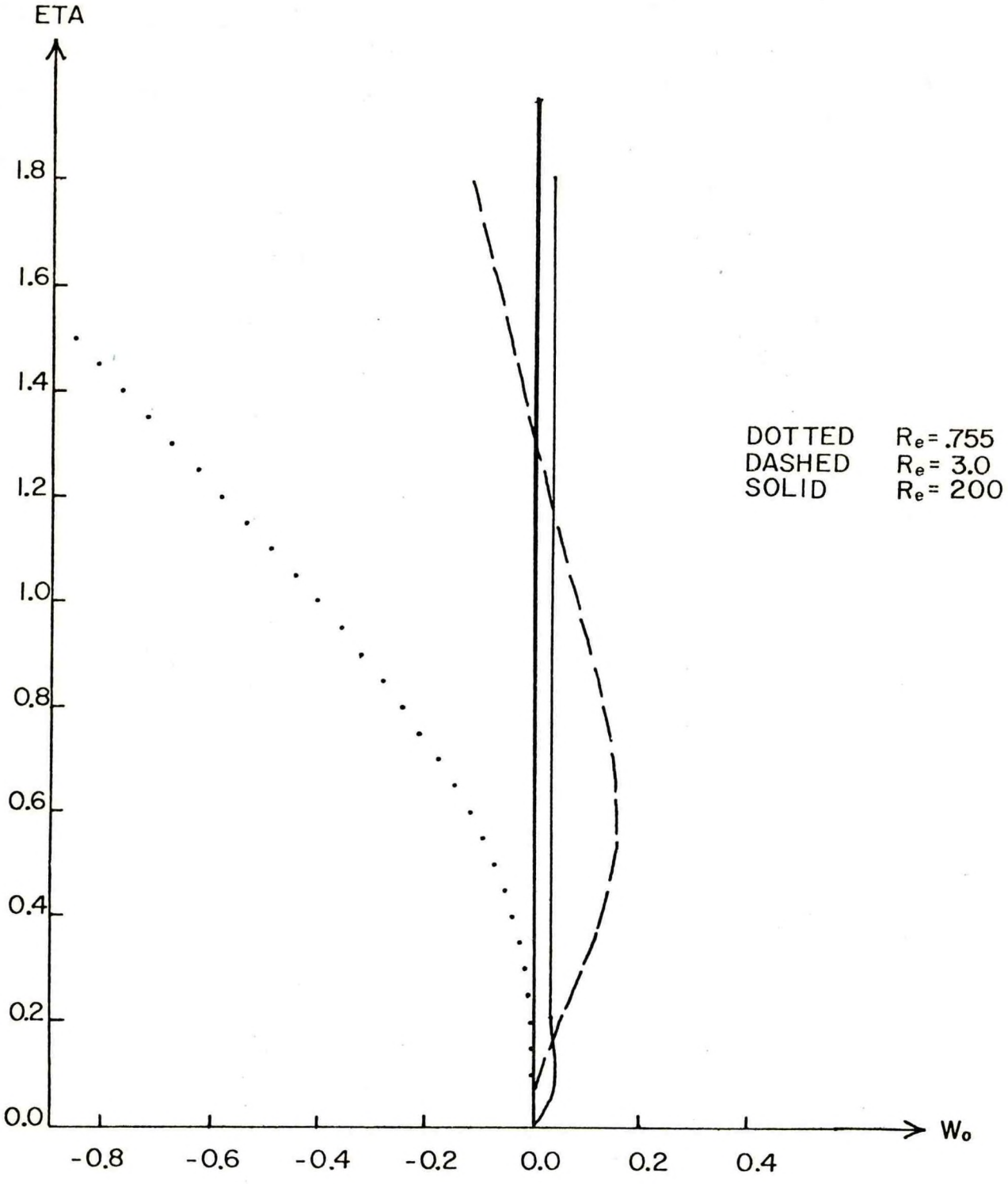
ETA
1.8
1.6
1.4
1.2
1.0
0.8
0.6
0.4
0.2
0.0
-0.8
-0.6
-0.4
-0.2
0.0
0.2
0.4
W_o
DOTTED $R_e = .755$
DASHED $R_e = 3.0$
SOLID $R_e = 200$

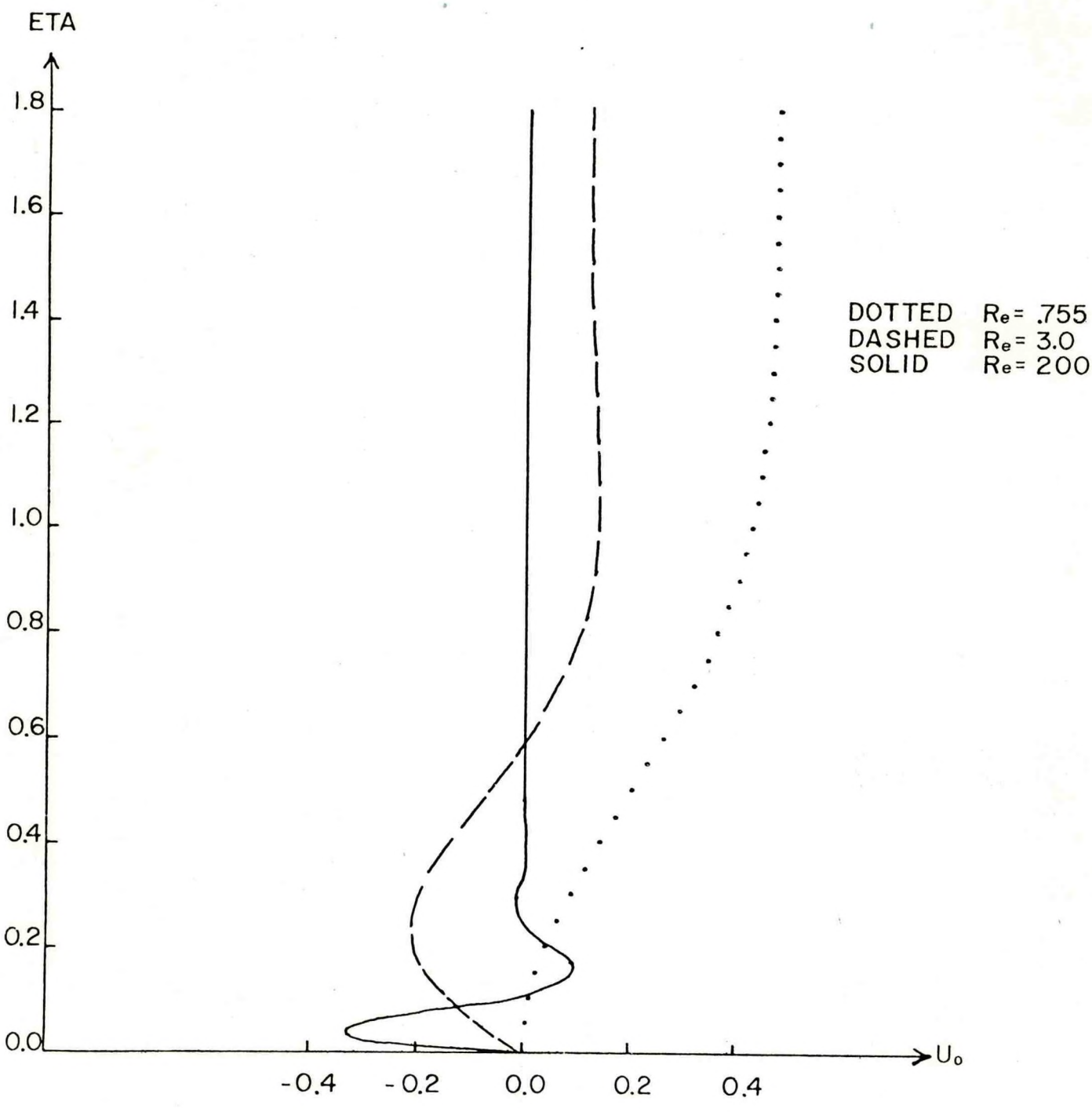
ETA
1.8
1.6
1.4
1.2
1.0
0.8
0.6
0.4
0.2
0.0
-0.4
-0.2
0.0
0.2
0.4
U_o
DOTTED R_e = .755
DASHED R_e = 3.0
SOLID R_e = 200

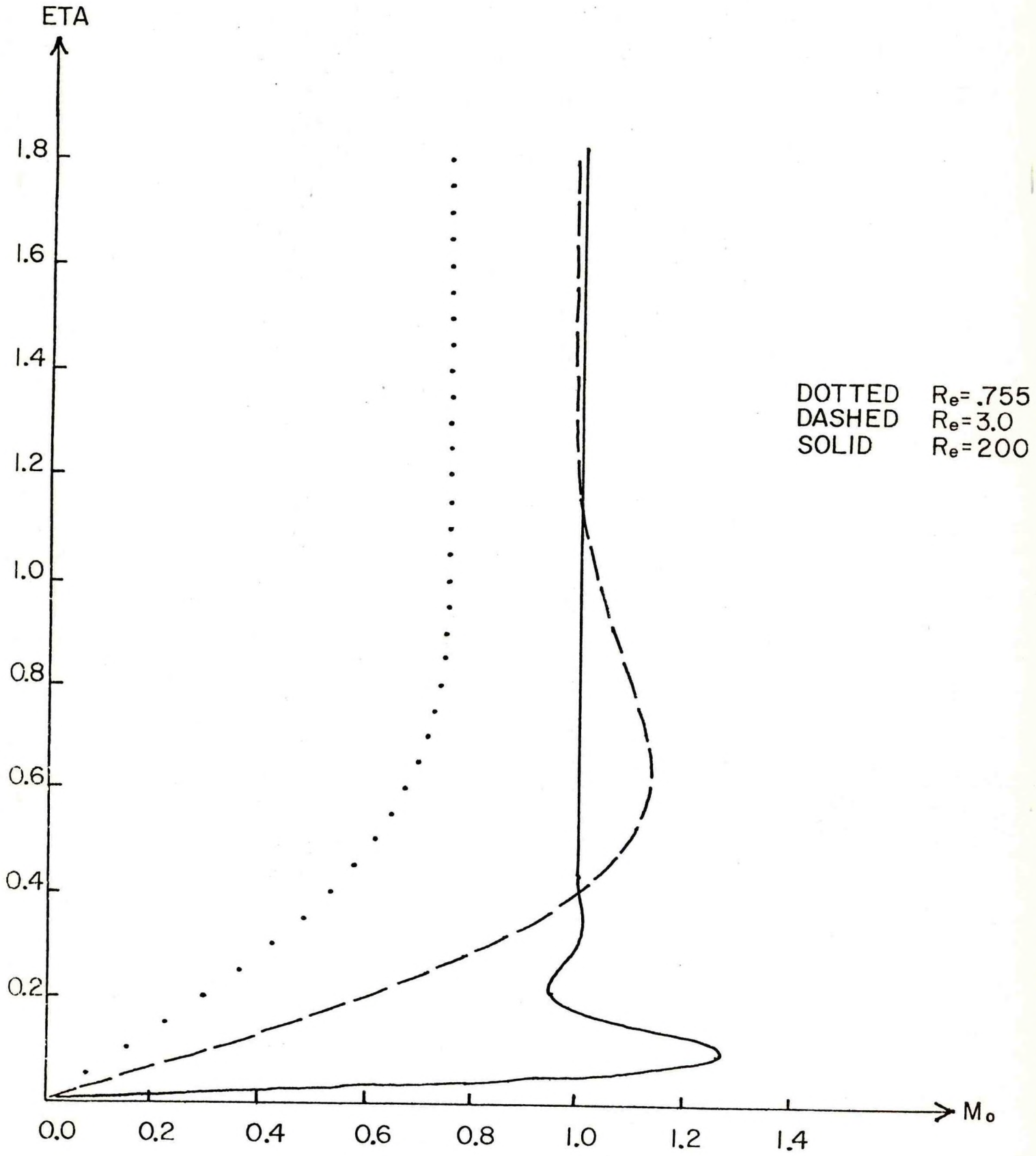
ETA
1.8
1.6
1.4
1.2
1.0
0.8
0.6
0.4
0.2
0.0
0.2
0.4
0.6
0.8
1.0
1.2
1.4
Mo
DOTTED Re=.755
DASHED Re=3.0
SOLID Re=200

PART III: AN INVESTIGATION OF THE BOUNDARY LAYER DYNAMICS OF A NON-STEADY AXISYMMETRIC MESOSCALE VORTEX

by

W. H. Raymond
Dept. of Earth and Atmospheric Sciences
Saint Louis University

TABLE OF CONTENTS

Abstract

In this study we examine the boundary layer dynamics of an idealized axisymmetric nonsteady vortex, extending the steady-state theories of Kuo (1971). The resulting nonlinear partial differential equations are then solved by the application of a Galerkin technique. Because of insufficient knowledge about atmospheric velocity profiles within the developing vortex we choose simplified initial conditions which contain nonzero tangential or tangential and vertical motions only. We then observe the production of secondary radial and vertical motions created by the nearly impulsive application of 'no-slip' boundary conditions. This time dependent Taylor boundary condition causes the fluid to decelerate or spin-down. During this process inertial oscillations are generated.

Our numerical calculations indicate that steady-state solutions are obtained when the deceleration is gradual. Speeding up the deceleration process gives rise to a large amplitude oscillatory vertical velocity. An analysis of the linearized equations indicates the presence of inertial oscillations of frequence $2(n)^{\frac{1}{2}}\Omega$, Ω the angular velocity and n a parameter, $0 \leq n \leq 1$. Numerical solutions suggest nearly similar conclusions. By comparing solutions of the nonlinear equations against linearized versions of the same equations we conclude that initially the vortex develops almost linearly. To verify the accuracy of our numerical procedure, comparisons between the Galerkin solutions for various time and space mesh sizes are made.

1. Introduction

The presence of vortices in our surroundings has sparked many inquiries into the nature of rotating fluids. In a theoretical setting the motions above or between rotating plates were the first to be analyzed, e.g., von Karman (1921). Later, Boedewadt (1940) studied the boundary layer dynamics of a vortex. Since then numerous investigations have been made broadening the subject area, e.g., analyzing the effects of non-solid rotation and geophysical boundary conditions. To a large extent most of these studies were concerned with the steady-state problem. The boundary layer dynamics of a developing vortex are more difficult to examine but are of special meteorological value.

The non-steady boundary layer dynamics of a rigidly rotating fluid have been studied by Thiriot (1940, 1950). By suddenly arresting the motion of a rotating disk in a viscous incompressible fluid he observed a time dependent boundary layer flow whose final state of motion (before deterioration) corresponded to the state predicted by Boedewadt (1940). An accelerating or decelerating disk has also been considered by Thirlot (1942). The related problem for the time-dependent flows between or above rotating disks have been examined by Pearson (1965), Benton (1966) and Florent et al. (1973). Experiments have also been conducted by Bode et al. (1975) in which a vortex is driven by a body force located along part of the axis of rotation. Although their study deals primarily with the effects of lower boundary conditions the evolution of the vortex was also examined.

In this study we extend Kuo's (1971) vortex model to the time domain. This vortex model assumes a power-law velocity distribution proportional to r^{2n-1}, $0 \leqslant n \leqslant 1$, r a radial measure (n = 1 corresponds to solid rotation and n = 0 implies potential flow). In this manner the governing Navier-Stokes equations are transformed into a system consisting of two parabolic and one first order partial differential equations. This system is solved by the variational technique known as the Galerkin method.

The characteristics of a non-steady vortex as it tends toward steady-state were first analyzed rigorously (in the classical spin-up problem) by Greenspan and Howard (1963). They showed that the spin-up takes place in three different time scales. Similarly, Benton (1966) has identified three distinct phases or growth patterns within the boundary layer for flow over an impulsively started disk. The first phase consisted of the boundary layer growing proportionally with time. During the second phase this growth slowed while the final phase consisted of a small amplitude decaying inertial oscillation about the steady state. We will try to identify various phases from our numerical solutions. The presence and importance of inertial oscillations are also discussed for both non-linear and linearized problems.

Atmospheric phenomena are difficult to model because of the involved physical and dynamical processes and lack of general knowledge of the transient radial pressure gradient

and its relationship to the tangential velocity, especially at the top of a growing boundary layer. However, there is some hint that mesometeorological vortices develop far above the earth's surface (e.g., 3 km) and then later slowly descend and appear near the surface (Brandes, 1977). Thus secondary velocity components are created because of the 'no-slip' lower boundary conditions and these motions interact as the fluid undergoes some boundary induced spin-down. The most striking example of this is the descent of a tornado to the earth's surface. To gain some knowledge of how the vortex boundary layer develops during spin-down we will investigate the dynamics of a very simple idealized situation similar to that considered by Thirlot (1940, 1942, 1950) but include both solid and non-solid rotations.

A fluid having an initial rotating horizontal motion or such a motion with superimposed vertical motion, is allowed to decelerate and approach the no-slip flow conditions at the lower boundary. This is accomplished by impulsively subjecting the tangential velocity to a time dependent geophysical boundary condition. Inertial oscillations are thereby generated. Their impact upon the growing boundary layer depends upon the impulsiveness of this deceleration process. Furthermore, the suddenness of this impulsive motion produces an initial boundary singularity. But the long term time dependent effects of such discontinuities on a diffusion equation (parabolic problem) are

usually small provided a fine mesh is used along with a stable difference method (Ames, 1969). Galerkin methods provide an alternative to such an approach.

Our conclusions show that the steady-state solutions were obtained without difficulty provided the deceleration was not too sudden. Speeding up the deceleration process enhanced the generation of inertial oscillations thereby giving rise to a large amplitude oscillatory vertical velocity. An analysis of the linearized equations shows a preferred frequency of $2(n)^{\frac{1}{2}}\Omega$ of the inertial oscillations. For solid rotation ($n = 1$) the frequency is simply 2Ω agreeing with Grenspan and Howard (1963) and Benton (1966). Thus, for non-solid rotation ($n<1$) this frequency becomes small. Results of the numerical solution of the non-linear equation also suggest similar conclusions.

2. Statement of the Problem

A. Nondimensionalization

The simplified time dependent governing set of partial differential equations are obtained by extending the concepts and transformations outlined by Kuo (1971) in his study of the boundary layer of an axisymmetric vortex in a steady-state. The Navier-Stokes equations are first simplified by assuming that variations along the boundary are much smaller than variations normal to the boundary. Next they are nondimensionalized. Representing dimensional variables with a bar and denoting nondimensional variables by ordinary letters, we set

$$\bar{v} = V_m v , \qquad \bar{u} = V_m u , \qquad \bar{w} = \frac{V_m \delta_R}{r_m} w ,$$

$$\bar{p} = V_m^2 \bar{\rho} p , \qquad \bar{r} = r_m r , \qquad \bar{z} = \delta_R z ,$$

$$\bar{t} = \frac{r_m}{V_m} \tilde{t} \quad \text{and} \quad \bar{\nu} = \frac{V_m \delta_R^2}{r_m} \nu ,$$

where V_m, r_m and δ_R are the maximum tangential velocity, horizontal scale length, and reference boundary layer thickness, respectively. The governing equations are:

$$\frac{\partial u}{\partial \tilde{t}} + u\frac{\partial u}{\partial r} + w\frac{\partial u}{\partial z} - \frac{v^2}{r} = -\frac{\partial p}{\partial r} + \nu\frac{\partial^2 u}{\partial z^2} ,$$

(1a)

$$\frac{\partial v}{\partial \tilde{t}} + u\frac{\partial v}{\partial r} + w\frac{\partial v}{\partial z} + \frac{uv}{r} = \nu\frac{\partial^2 v}{\partial z^2} ,$$

$$\frac{\partial u}{\partial r} + \frac{u}{r} + \frac{\partial w}{\partial z} = 0. \qquad (1b)$$

B. The Similarity Transformations

We now simplify the above equations utilizing the following similarity transformations suggested by Kuo (except for t):

$$z = \delta\eta, \qquad \tilde{t} = \frac{\delta^2}{r}t, \qquad \frac{\partial p}{\partial r} = r^{4n-3},$$

$$\delta = r^{1/2}r^{1-n}, \quad u = -r^{2n-1}F(\eta,t), \quad v = r^{2n-1}G(\eta,t) \qquad (1c)$$

$$\text{and} \quad w = \left[(n+1)H(\eta,t) + (n-1)\eta F(\eta,t)\right] r^{n-1}r^{1/2}.$$

Furthermore the above horizontal velocity transformations can be related to the angular momentum m through

$$v = m/r = m_o G/r \text{ and } u = -m_o F/r,$$

where $m_o = r^{2n}$ (a power law distribution).

It is clear that even though the velocity distribution of a vortex cannot be 'continuously' represented by such a power-law with a fixed value of n , it is however possible to represent various parts of the vortex for different values of n. Very close to the axis the flow is in solid rotation which corresponds to n = 1. Outside the region of maximum winds the velocity components become proportional to 1/r satisfying the well known potential vortex relationship which corresponds to n = 0. Unfortunately, steady-state solutions do not exist for n's much smaller than 0.5. For any fixed n the similarity solution would be valid for a limited range of r provided the solution exists and behaves properly.

Equations (1a) and (1b) become respectively (2a) and (2b) when (1c) is utilized:

$$\frac{\partial F}{\partial t} + (1-2n)F^2 + (n+1)H\frac{\partial F}{\partial \eta} + G^2 - 1 = \frac{\partial^2 F}{\partial \eta^2}, \tag{2a}$$

$$\frac{\partial G}{\partial t} - 2nFG - (n-1)H\frac{\partial G}{\partial \eta} = \frac{\partial^2 G}{\partial \eta^2},$$

$$F = \frac{\partial H}{\partial \eta}. \tag{2b}$$

The formulation of the above problem is completed by specifying the initial and boundary conditions.

C. Initial and boundary conditions

The growth of the boundary layer during the spin-down of a vortex in uniform rotation is of special interest in this study. We require initial conditions of the form

$$F(\eta,0) = 0,$$
$$G(\eta,0) = 1, \tag{2c}$$
and $$H(\eta,0) = h_o.$$

For the lower boundary at $\eta = 0$ we require that the radial component be zero while the tangential component slowly decelerates, resulting in

$$F(0,t) = 0,$$
$$G(0,t) - K(t)\frac{\partial G(0,t)}{\partial \eta} = 0, \quad t>0, \tag{2d}$$
and $$H(0,t) = h_1(t).$$

We choose a coefficient K(t) of the form $K(t) = \sigma \exp(-t/\sigma)$, σ a positive constant. Note the K(t) rapidly approaches

zero with increasing value of t. A constant K implies the employment of the geophysical boundary condition (Taylor, 1915).

For the upper boundary conditions at $\eta = \delta_\eta$ we have

$$F(\delta_\eta, t) = 0,$$
$$G(\delta_\eta, t) = 1. \qquad (2e)$$

Because the boundary layer thickness varies with time, selecting the steady-state value δ_η insures an adequate depth for the calculations.

The initial boundary singularity at $\eta = 0$ and $t = 0$ arises because, from (2c)

$$1 = \lim_{t \to 0} G(0,t) \neq \lim_{t \to 0} K(t) \frac{\partial G(0,t)}{\partial \eta} = 0.$$

By examing a range of values for K(t) we can study the effect within a vortex imposed by the discontinuous initial boundary condition, e.g., inertial oscillations can be generated in this manner. Larger values for K(t) imply that a smaller impulsive change in $\partial G/\partial \eta$ and/or G is required at the first discrete time step in the numerical procedure. We do require that $h_o = \lim_{t \to 0} h_1(t)$.

An analytical evaluation of the effects of the initial boundary discontinuity is difficult to obtain because of the nonlinearity of the equations. The normal numerical procedure is to vary the grid mesh and observe the resulting changes and

compare for special cases the numerical approximation with known solutions. Both of these techniques will be used in this study.

C. The Linearized Problem

To isolate the contribution of the nonlinear terms during early stages of the boundary layer development, we will analyze a system of linearized equations. These are obtained by expanding F, G and H in powers of a small parameter ϵ, i.e.,

$$\begin{aligned} F(\eta, t) &= \sum_{k=1}^{\infty} \epsilon^k f_k , \\ G(\eta, t) &= 1 + \sum_{k=1}^{\infty} \epsilon^k g_k , \\ H(\eta, t) &= \sum_{k=1}^{\infty} \epsilon^k h_k + h_o , \end{aligned} \tag{3}$$

where $f_k = f_k(\eta, t)$, $g_k = g_k(\eta, t)$ and $h_k(\eta, t)$, and substituting them into (2a, b). This yields, after simplification, the following system of linear equations:

$$\begin{aligned} \frac{\partial f_k}{\partial t} + (n+1) h_o \frac{\partial f_k}{\partial \eta} + 2 g_k - \frac{\partial^2 f_k}{\partial \eta^2} &= -(1-2n) \sum_{j=1}^{k-1} \epsilon^{k-j-1} f_{k-j} f_j \\ &\quad - (n+1) \sum_{j=1}^{k-1} \epsilon^{k-j-1} h_{k-j} \frac{\partial f_j}{\partial \eta} - \sum_{j=1}^{k-1} \epsilon^{k-j-1} g_{k-j} g_j , \end{aligned} \tag{4a}$$

$$\begin{aligned} \frac{\partial g_k}{\partial t} + (n+1) h_o \frac{\partial g_k}{\partial \eta} - 2n f_k - \frac{\partial^2 g_k}{\partial \eta^2} &= 2n \sum_{j=1}^{k-1} \epsilon^{k-j-1} f_{k-j} g_j \\ &\quad - (n+1) \sum_{j=1}^{k-1} \epsilon^{k-j-1} h_{k-j} \frac{\partial g_j}{\partial \eta} , \end{aligned}$$

$$\frac{\partial h_k}{\partial \eta} = f_k . \tag{4b}$$

The initial conditions (2c) become

$$f_k(\eta,0) = 0,\ k \geq 1,$$

$$g_k(\eta,0) = 0, \tag{4c}$$

and $$h_k(\eta,0) = 0$$

while the boundary conditions (2d) require that

$$\left.\begin{aligned} f_k &= 0 \\ h_k &= 0 \end{aligned}\right\} k \geq 1,$$

$$1 + g_1 = K(t)\,\frac{\partial g_1}{\partial \eta}, \tag{4d}$$

$$g_k = K(t)\,\frac{\partial g_k}{\partial \eta},\ k > 1.$$

At the top of the boundary layer we have that

$$f_k(\delta_\eta, t) = 0$$

$$g_k(\delta_\eta, t) = 0,\ k \geq 1. \tag{4e}$$

For convenience, follow Kuo (1971) and set $\epsilon = 1$.

3. An Analysis of the Linear Problem for Inertial Oscillations

The presence of inertial oscillations in fluids undergoing spin-up or spin-down has been carefully documented, see Greenspan and Howard (1963), Benton (1966) and Debnath and Mukherjee (1974). For a homogeneous fluid in solid rotation these oscillations exhibit a frequency of twice the angular velocity Ω. For flow over a rotating disk Benton (1966) indicates that, in the very least, inertial oscillations are responsible for overshoot since a damped oscillation of frequency 2Ω appears as the fluid approaches the steady-state. Greenspan and Howard (1963) have pointed out that in the earlier stages of motion development inertial oscillations contribute to the same extent as other terms.

In our problem we examine the characteristics of inertial oscillations by analytically analyzing the linear equations (4a) and (4b). Assuming $k = 1$ and $h_o = 0$ we obtain the homogeneous system

$$\frac{\partial f_1}{\partial t} + 2g_1 = \frac{\partial^2 f_1}{\partial \eta^2}, \qquad (5)$$

$$\frac{\partial g_1}{\partial t} - 2\eta f_1 = \frac{\partial^2 g_1}{\partial \eta^2}.$$

Provided a solution of the form

$$f_1 = f_o e^{-i\gamma t}, \qquad (6)$$

$$g_1 = g_o e^{-i\gamma t},$$

exists, then it can be shown that the solutions for f_1 and g_1 approach zero as η approaches infinity, regardless of

the lower boundary conditions, provided the characteristic roots of

$$m^4 + 2i\gamma m^2 - \gamma^2 + 4n = 0,$$

have negative real parts. Rewriting the characteristic equation in terms of two equations in p and q when m = p + iq, p and q real numbers, gives

$$(p^2 + q)^2 - 2pq(4pq + 2\gamma) - \gamma^2 + 4n = 0,$$

$$(4pq + 2\gamma)(p^2 - q^2) = 0.$$

After some algebra it can be shown that p is negative and real provided $|\gamma| > 2(n)^{\frac{1}{2}}$. Note, for non-zero values of h_o the above frequency must be modified. Debnath and Mukherjee (1974) have discussed this point for flow over a rotating disk.

When $\gamma = 2(n)^{\frac{1}{2}}$, f_1 and g_1 exhibit only pure inertial oscillation. When γ is related back to a dimensional variable, say $\bar{\gamma}$, the frequency is $\bar{\gamma} = 2(n)^{\frac{1}{2}}\Omega$. Here Ω ($\Omega = \frac{v_m}{r_m} r^{2n-2}$ in our model) is the dimensional angular velocity at the top of the boundary layer. For solid rotation (n = 1) this is in agreement with Greenspan and Howard (1963). For non-solid rotation (n < 1) this frequency is reduced. We now examine the numerical solution of the full non-linear equations and make comparisons with these results.

4. Discussion of Results

The strength and vitality of the secondary velocity components are good measures of the development of the boundary layer. The variations in the radial component, F-field, for the nondimensional times T = 1.6, 7.2, 16, 56 respectively are shown in Figure 1 for n = 1.0 (solid rotation) and for $K = 5e^{-T/5}$. During this time interval the K-variation was from 3.63 to 0. In these calculations as in most, unless otherwise stated, we selected the nondimensional time step $\Delta t = 0.04$ and the grid distance h = 0.15. The most significant feature shown in Figure 1 is that the radial component develops rapidly an inward motion near the surface, e.g., when T = 1.6, then slowly builds (for larger T's) vertically until damped sinusoidual motions typical of steady-state solutions are obtained. Moderate growth of the lower inflow layer occurs between T = 1.6 and 16 after which additional development is somewhat subdued. By T = 30 (not shown) the velocity component deviated by less than 1% from the steady-state value. As time T approaches 56 there is a very small damped oscillation about the steady-state value similar to the behavior described by Benton (1966). The almost negligible deviation at time T = 56 from Kuo's steady-state values is illustrated in Table 1.

Figure 2 shows the changes in the radial component at T = 2, 10, 20, 29, 56 when n = 0.5 (non-solid rotation) and for $K = 6e^{-T/6}$. The larger time dependent value of K was chosen

to facilitate a visual appreciation of the growth pattern. As before the radial component contains only inflow (T = 2) during early development but by T = 10 there is both inflow and outflow in the vertical. This damped oscillation pattern progresses vertically until near steady-state values are obtained at T = 56.

In Figure 3 the dimensionless tangential velocity component G is illustrated at T = 2, 8, 16, 56 for non-solid rotation (n = 0.75) and when $K = 5e^{-T/5}$. An important physical feature is the existence of G values larger than those demanded under a cyclostrophic balance condition for all values of T near $\eta \sim 4$. The time required to reach steady-state conditions was commensurate with those when n = 1.0 using the same expression for K.

A comparison between the radial components when n = 1 (solid rotation) and n = 0.5 (non-solid rotation) at fixed times T = 4 and 16 is made in Figure 4. The rapid growth of the F profile for non-solid rotation is apparent since at either time these profiles are over 50% larger, in the vertical direction, than their n = 1 counterparts. Such a percentage difference is evident for larger T's also when near steady-state conditions prevail.

Profiles resembling those in Figure 4 may be obtained by adding mass to the system, i.e., by applying a small non-negative vertical velocity (blowing or sucking), say $h_1(t) = h_o$, a constant, at the lower boundary. In Figure 5 we illustrate

the dimensionless radial component F when $h_o = 0.2$ and $h_o = 0$. From these (and other calculations not shown) we conclude that blowing amplifies the boundary layer thickness, speeds up its growth rate, and causes the vortex to behave similar to a vortex having a more non-solid rotation. These conclusions are compatible with those reached by analyzing the effects of blowing in the steady-state problem.

Modifying the value of K has a pronounced effect upon the velocity distribution because of the possible enhancement of inertial oscillations. This is best illustrated by studying changes in the vertical velocity H and the radial component F. In Figure 6 the temporal change in H at the top of the boundary layer of a vortex in non-solid rotation (n = 0.5) is plotted for a range of values of K generated by the expression:

$$K(t) = \sigma \exp(-t/\sigma)$$

where $\sigma = 1, 3, 5$ and 10.

We identify two major flow characteristics from Figure 6. The first is that the value of H at the top of the boundary layer experiences rapid changes in magnitude with variations in σ. The other feature is the quasi-oscillatory behavior of H particularly for the smaller σ's. These variations in H are due to inertial oscillations which become very predominate for the smaller values of σ, a nearly impulsive application or the no-slip boundary condition. No stationary flow could be achieved within the allotted computer time of ten minutes on the C.D.C. 7600 with $\sigma = 0$.

The period, $2\pi/\gamma$, of these oscillations, as evident in Figures 6 and 7, for n = 0.5 is very nearly 4.4 $\pm$ 0.2 non-dimensional time units. This agrees well with the value 4.443 predicted from the linear analysis in Section 3. Similar analysis for n = 1.0 shows an oscillation period very nearly equal to the predicted value of π.

The variation in the depth of the surface inflow layer ($F > .005$) as a function of n and time is shown in Figure 8. The differences in the magnitude and oscillatory behavior is directly related to the n variation.

Solutions of the linear problem, equations (4a) and (4b), are obtained by Galerkin methods in an identical manner to that described above except that the predictor-corrector procedure was not necessary. Our resulting numerical calculations for H at times T = 15 and T = 33 are shown in Figures 9 and 10, respectively. In each figure three profiles are shown representing the power series solutions containing the first term; the first plus the second term; and all terms, respectively. The latter is the solution of the non-linear problem described by equations (2a) and (2b). For simplicity in the linearization process we have taken $\epsilon = 1.0$, following Kuo (1971). Figure 9 shows clearly that during early stages of the vortex development the contribution of the non-linear terms is small. However later, as evidenced by Figure 10 they are extremely important, especially in the lower three-fourths of the boundary

layer. Variations in K also affect the degree of linearity of the problem.

To expound further upon the accuracy of the Galerkin solutions, in addition to what was evident from Table 1, we altered the time step $\triangle t$ and grid spacing h to check our previous deductions. We present selected values of G for $\eta = 0$ and F for various η's in Tables 2, 3 and 4 for T's 1.6 and 8.0. Note that the value of F and G in Tables 2 and 3 is changed very little as a result of changing $\triangle t$. We emphasize that the differences between the respective values of F and G calculated using the time steps $\triangle t = 0.02$, 0.04 and 0.08 are reduced as $\triangle t$ becomes smaller, indicating that convergence is taking place. Likewise changing the space interval h gives similar results as shown in Table 4. This technique, a standard one for testing numerical solutions of partial differential equations checks out the adequacy of the Galerkin method for our purposes.

5. Conclusions

In summary we note that the secondary flows developed in the boundary layer during the deceleration of a vortex exhibit quasi-oscillatory behavior due to inertial oscillations of frequency $\bar{\gamma} = 2(n)^{\frac{1}{2}}\Lambda$, $0 \leq n \leq 1$. For solid rotation, n = 1, these results agree with previous findings. In non-solid rotation, $n < 1$, the frequency is reduced. When nearly impulsive boundary conditions are applied, e.g., $\sigma = 1$, these inertial oscillations create a large oscillatory vertical velocity. By varying $\triangle t$ and space interval h it is confirmed that these large vertical velocities are physically real and do not arise from an inaccuracy in our numerical (Galerkin) procedure. Linear analysis (Section 3) confirms the frequency and period of these inertial oscillations. Under impulsive conditions, $\sigma = 0$, convergence could not be attained.

Our analysis showed that the radial component rapidly developed an inward motion near the lower surface. The sinuosoidual growth in the vertical then proceded at a slower rate. Finally, there existed a small amplitude decaying oscillation, of frequnecy $\bar{\gamma} = 2(n)^{\frac{1}{2}}\Lambda$ ($\Lambda = \frac{v_m}{r_m} r^{2n-2}$), about the steady state provided the flow showed a tendency to converge. These phases in the growth of the boundary layer are somewhat similar to those described by Benton (1966). We showed further that in the early stages the boundary layer development is essentially linear with nonlinear terms becoming important later.

To analyze further the transient boundary layer dynamics of an atmospheric vortex it would be necessary to know accurately the relationship between the radial pressure gradient and the tangential velocity component at the top of the boundary layer. An accurate formulation of the wind-pressure relationship is not easy because of the lack of measurements. In addition to this relationship, a study incorporating other physically important quantities, such as the effect of thermodynamics, the effect of the release of latent heat, and the inclusion of turbulence, would greatly refine and improve our knowledge of the atmospheric vortices.

ACKNOWLEDGMENTS

This research is sponsored jointly by Grant No. 04-06-022-4403 of the National Severe Storms Laboratory and ATM 74-09448-A02 of the National Science Foundation (Principal Investigator: Professor Y. J. Lin). Deep appreciation is expressed to Professors G. V. Rao and A. Garder for their advice during the progress of this study.

APPENDIX A

Adoption of the Galaxin Method for the Boundary Layer Problem

Equations (2a, b, c, d, e) describe a nonlinear initial-boundary value problem. Nonlinear problems are customarily solved numerically. Recent advances in a numerical technique known as the Galerkin method have been outlined by Ciarlet et al. (1967), Douglas and Dupont (1970) and Wang et al. (1972). Advantages of the Galerkin method over finite difference methods have been noted in these, and in other recent publications, e.g., Swartz and Wendroff (1974). We now proceed with our development of the Galerkin method.

The variational form of (2a, b) is obtained by multiplying each equation by $V(\eta)$ and integrating with respect to η from 0 to δ_η, yielding

$$\int_0^{\delta_\eta} \left[\frac{\partial F}{\partial t} + (n+1)H\frac{\partial F}{\partial \eta} - \frac{\partial^2 F}{\partial \eta^2} + (1-2n)F^2 + G^2 - 1\right] V(\eta)\,d\eta = 0,$$

$$\int_0^{\delta_\eta} \left[\frac{\partial G}{\partial t} + (n+1)H\frac{\partial G}{\partial \eta} - \frac{\partial^2 G}{\partial \eta^2} - 2nFG\right] V(\eta)\,d\eta = 0, \qquad \text{(A1)}$$

$$\int_0^{\delta_\eta} \left[\frac{\partial H}{\partial \eta} - F\right] V(\eta)\,d\eta = 0. \qquad \text{(A2)}$$

The above integrals, along with the initial conditions, must be satisfied for those $V(\eta)$ that belong to the set S of real-valued functions that are piecewise continuously differentiable on $[0, \delta_\eta]$. The Galerkin approximations to F, G and H will be represented by F, G and H, respectively, which belong to a

finite dimensional subspace, M, of S. Ciarlet et al. (1967) considered several possible choices for M from which we choose the chapeau functions because they lead to a tridiangonal matrix.

The interval $[0, \delta_\eta]$ is subdivided into units of constant length $h = \eta_{j+1} - \eta_j$ by the partition

$$0 = \eta_1 < \cdots < \eta_N = \delta_\eta .$$

The subspace M is defined by the basis $\{V_j\}$, where

$$V_1 = \begin{cases} (\eta_2 - \eta)/h , & \eta_1 \le \eta \le \eta_2 , \\ 0 , & \text{otherwise,} \end{cases}$$

$$V_j = \begin{cases} (\eta - \eta_{j-1})/h , & \eta_{j-1} \le \eta \le \eta_j , \\ (\eta_{j+1} - \eta)/h , & \eta_j \le \eta \le \eta_{j+1} , \\ 0 , & \text{otherwise,} \end{cases}$$

$$V_N = \begin{cases} (\eta - \eta_{N-1})/h , & \eta_{N-1} \le \eta \le \eta_N , \\ 0 , & \text{otherwise.} \end{cases}$$

The coefficients in the Galerkin approximations are defined by substituting

$$\begin{aligned} \bar{F}(\eta, t) &= \sum_{i=1}^{N} \alpha_i(t) V_i(\eta) , \\ \bar{G}(\eta, t) &= \sum_{i=1}^{N} \beta_i(t) V_i(\eta) , \\ \bar{H}(\eta, t) &= \sum_{i=1}^{N} \gamma_i V_i(\eta) , \end{aligned} \qquad \text{(A3)}$$

for F, G and H in (A1, A2), and $V_j(\eta)$ for $V(\eta)$. It is to be noted that $V_1(0) = 1$, $V_N(\delta_\eta) = 1$ and each of the approximations

do not yet satisfy the required boundary conditions. The implementation of the boundary conditions will be considered later. (A1, A2) is now represented by the following system of equations

$$\int_0^{\delta_\eta} \frac{\partial F}{\partial t} V_j d\eta + (n+1)\int_0^{\delta_\eta} H \frac{\partial F}{\partial \eta} V_j d\eta - \int_0^{\delta_\eta} \frac{\partial^2 F}{\partial \eta^2} V_j d\eta + (1-2n)\int_0^{\delta_\eta} F^2 V_j d\eta + \int_0^{\delta_\eta} G^2 V_j d\eta - \int_0^{\delta_\eta} V_j d\eta = 0,$$

(A4)

$$\int_0^{\delta_\eta} \frac{\partial G}{\partial t} V_j d\eta + (n+1)\int_0^{\delta_\eta} H \frac{\partial G}{\partial \eta} V_j d\eta - \int_0^{\delta_\eta} \frac{\partial^2 G}{\partial \eta^2} V_j d\eta - 2n\int_0^{\delta_\eta} FG V_j d\eta = 0,$$

and

$$\int_0^{\delta_\eta} \frac{\partial H}{\partial \eta} V_j d\eta - \int_0^{\delta_\eta} F V_j d\eta = 0,$$

(A5)

where j = 1, . . . , N. Integration by parts given an equivalent representation, where for convenience we use the notation + in 0+ and - in δ_η^- to indicate approaching these limits from the right and left respectively,

$$\int_0^{\delta_\eta} \frac{\partial F}{\partial t} V_j d\eta + (n+1)\int_0^{\delta_\eta} H \frac{\partial F}{\partial \eta} V_j d\eta + \int_0^{\delta_\eta} \frac{\partial F}{\partial \eta} \frac{dV_j}{d\eta} d\eta + (1-2n)\int_0^{\delta_\eta} F^2 V_j d\eta + \int_0^{\delta_\eta} G^2 V_j d\eta - \int_0^{\delta_\eta} V_j d\eta - \frac{\partial F}{\partial \eta} V_j\Big|_{\delta_\eta^-} + \frac{\partial F}{\partial \eta} V_j\Big|_{0^+} = 0,$$

(A6)

$$\int_0^{\delta_\eta} \frac{\partial G}{\partial t} V_j d\eta + (n+1)\int_0^{\delta_\eta} H \frac{\partial G}{\partial \eta} V_j d\eta + \int_0^{\delta_\eta} \frac{\partial G}{\partial \eta} \frac{dV_j}{d\eta} d\eta - 2n\int_0^{\delta_\eta} FG V_j d\eta - \frac{\partial G}{\partial \eta} V_j\Big|_{\delta_\eta^-} + \frac{\partial G}{\partial \eta} V_j\Big|_{0^+} = 0,$$

$$\int_0^{\delta_\eta} \frac{\partial H}{\partial \eta} V_j \, d\eta - \int_0^{\delta_\eta} F V_j \, d\eta = 0. \qquad \text{(A7)}$$

Applying (A3), simplifying, and writing in matrix notation, we obtain

$$\begin{aligned} A\frac{d\vec{\alpha}}{dt} + B_1(\vec{\alpha},\vec{\gamma})\vec{\alpha} + C(\vec{\beta})\vec{\beta} + \vec{J} &= 0, \\ A\frac{d\vec{\beta}}{dt} + B_2(\vec{\gamma})\vec{\beta} - 2nC(\vec{\beta})\vec{\alpha} &= 0, \\ B_3\vec{\gamma} - A\vec{\alpha} &= 0, \end{aligned} \qquad \text{(A8)}$$

where

$$\begin{aligned} \vec{\alpha}^T &= [\alpha_1, \alpha_2, \ldots, \alpha_N], \\ \vec{\beta}^T &= [\beta_1, \beta_2, \ldots, \beta_N], \\ \vec{\gamma}^T &= [\gamma_1, \gamma_2, \ldots, \gamma_N], \end{aligned}$$

and

$$A = [a_{ji}], \quad a_{ji} = \int_0^{\delta_\eta} V_i V_j \, d\eta ;$$

$$B_1(\vec{\alpha},\vec{\gamma}) = [b_{1ji}], \quad b_{1ji} = \int_0^{\delta_\eta} \Big(\sum_{L=1}^{N} (n+1)\gamma_L V_L V_i' V_j + V_i' V_j' + \sum_{L=1}^{N} (1-2n)\alpha_L V_L V_i V_j \Big) d\eta - V_i' V_j \Big|_{\delta_\eta^-} + V_i' V_j \Big|_{0^+} ;$$

$$B_2(\gamma) = [b_{2ji}], \quad b_{2ji} = \int_0^{\delta_\eta} \Big(\sum_{L=1}^{N} (n+1)\gamma_L V_L V_i' V_j + V_i' V_j' \Big) d\eta - V_i' V_j \Big|_{\delta_\eta^-} + V_i' V_j \Big|_{0^+} ;$$

$$B_3 = \left[b_{3ji}\right], \quad b_{3ji} = \int_0^{\delta_\eta} V_i' V_j \, d\eta \; ;$$

$$C(\vec{\beta}) = \left[c_{ji}\right], \quad c_{ji} = \int_0^{\delta_\eta} \sum_{L=1}^{N} \beta_L V_L V_i V_j \, d\eta \; ;$$

$$\vec{d} = \left[d_j\right], \quad d_j = -\int_0^{\delta_\eta} V_j \, d\eta \; ; \quad \text{and } V_i' = \frac{dV_i}{d\eta} .$$

The tridiagonal nature of the above matrices is illustrated by the following example representing matrices generated from linear and nonlinear terms, respectively. First we see that

$$A = \frac{h}{6}\begin{bmatrix} 2 & 1 & & & & & \\ 1 & 4 & 1 & & & & \\ & \ddots & \ddots & \ddots & & & \\ & & \ddots & \ddots & \ddots & & \\ & & & 1 & 4 & 1 & \\ & & & & 1 & 2 \end{bmatrix} ,$$

and for $E = \left[e_{ji}\right]$, $e_{ji} = \int_0^{\delta_\eta} \sum_{L=1}^{N} \gamma_L V_L V_i' V_j \, d\eta$, $i, j = 1, \cdots, N$;

$$E = \frac{1}{6}\begin{bmatrix} -(2\gamma_1+\gamma_2) & (2\gamma_1+\gamma_2) & & & \\ -(\gamma_1+2\gamma_2) & (\gamma_1-\gamma_3) & (2\gamma_2+\gamma_1) & & \\ & \ddots & \ddots & \ddots & \\ & & -(\gamma_{i-1}+2\gamma_i) & (\gamma_{i-1}-\gamma_{i+1}) & (2\gamma_i+\gamma_{i+1}) \\ & & & \ddots & \ddots \\ & & & -(\gamma_{N-2}+2\gamma_{N-1}) & (\gamma_{N-2}-\gamma_N) \\ & & & & -(\gamma_{N-1}+2\gamma_N) \end{bmatrix} .$$

Wang et al. (1972) suggested the following Crank-Nicolson method for discretizing the time domain (dimensionless t domain in our case). They also wrote the equations (A8) in terms of the differences of two time (t) steps to increase computational stability. Letting the superscript denote the t step we have

(A9)

$$\left(A+\frac{\Delta t}{2}B_1\left(\frac{\vec{\alpha}^{k+1}+\vec{\alpha}^{k}}{2},\frac{\vec{\gamma}^{k+1}+\vec{\gamma}^{k}}{2}\right)\right)\left[\vec{\alpha}^{k+1}-\vec{\alpha}^{k}\right]+$$
$$\frac{\Delta t}{2}C\left(\frac{\vec{\beta}^{k+1}+\vec{\beta}^{k}}{2}\right)\left[\vec{\beta}^{k+1}-\vec{\beta}^{k}\right]=\Delta t\vec{d}-\Delta t B_1\left(\frac{\vec{\alpha}^{k+1}+\vec{\alpha}^{k}}{2},\frac{\vec{\gamma}^{k+1}+\vec{\gamma}^{k}}{2}\right)\vec{\alpha}^{k}$$
$$-\Delta t C\left(\frac{\vec{\beta}^{k+1}+\vec{\beta}^{k}}{2}\right)\vec{\beta}^{k},$$

$$-n\Delta t C\left(\frac{\vec{\beta}^{k+1}+\vec{\beta}^{k}}{2}\right)\left[\vec{\alpha}^{k+1}-\vec{\alpha}^{k}\right]+\left(A+\frac{\Delta t}{2}B_2\left(\frac{\vec{\gamma}^{k+1}+\vec{\gamma}^{k}}{2}\right)\right)\left[\vec{\beta}^{k+1}-\vec{\beta}^{k}\right]$$
$$=2n\Delta t C\left(\frac{\vec{\beta}^{k+1}+\vec{\beta}^{k}}{2}\right)\vec{\alpha}^{k}-\Delta t B_2\left(\frac{\vec{\gamma}^{k+1}+\vec{\gamma}^{k}}{2}\right)\vec{\beta}^{k},$$

and

$$A\left[\vec{\alpha}^{k+1}-\vec{\alpha}^{k}\right]-B_3\left[\vec{\gamma}^{k+1}-\vec{\gamma}^{k}\right]=2B_3\vec{\gamma}^{k}-2A\vec{\alpha}^{k}.$$

To avoid the necessity of solving a nonlinear algebraic system a predictor-corrector scheme suggested by Douglas and Dupont (1970) is used to approximate (A9):

Predictor

$$\left(A + \frac{\Delta t}{2} B_1(\vec{\alpha}^k, \vec{\gamma}^k)\right)\left[\vec{\alpha}^{*k+1} - \vec{\alpha}^k\right] + \frac{\Delta t}{2} C(\vec{\beta}^k)\left[\vec{\beta}^{*k+1} - \vec{\beta}^k\right] = -\Delta t \vec{d}$$

$$- \Delta t B_1(\vec{\alpha}^k, \vec{\gamma}^k)\vec{\alpha}^k - \Delta t C(\vec{\beta}^k)\vec{\beta}^k ,$$

$$-n\Delta t C(\vec{\beta}^k)\left[\vec{\alpha}^{*k+1} - \vec{\alpha}^k\right] + \left(A + \frac{\Delta t}{2} B_2(\vec{\gamma}^k)\right)\left[\vec{\beta}^{*k+1} - \vec{\beta}^k\right] =$$

$$2n\Delta t C(\vec{\beta}^k)\vec{\alpha}^k - \Delta t B_2(\vec{\gamma}^k)\vec{\beta}^k ,$$

and

$$A\left[\vec{\alpha}^{*k+1} - \vec{\alpha}^k\right] - B_3\left[\vec{\gamma}^{*k+1} - \vec{\gamma}^k\right] = 2B_3\vec{\gamma}^k - 2A\vec{\alpha}^k ;$$

Corrector

$$\left(A - \frac{\Delta t}{2} B_1\left(\frac{\vec{\alpha}^{*k+1} + \vec{\alpha}^k}{2}, \frac{\vec{\gamma}^{*k+1} + \vec{\gamma}^k}{2}\right)\right)\left[\vec{\alpha}^{k+1} - \vec{\alpha}^k\right] + \frac{\Delta t}{2} C\left(\frac{\vec{\beta}^* + \vec{\beta}^k}{2}\right)\left[\vec{\beta}^{k+1} - \vec{\beta}^k\right]$$

$$= -\Delta t \vec{d} - \Delta t B_1\left(\frac{\vec{\alpha}^{*k+1} + \vec{\alpha}^k}{2}, \frac{\vec{\gamma}^{*k+1} + \vec{\gamma}^k}{2}\right)\vec{\alpha}^k - \Delta t C\left(\frac{\vec{\beta}^{*k+1} + \vec{\beta}^k}{2}\right)\vec{\beta}^k ,$$

$$-n\Delta t C\left(\frac{\vec{\beta}^{*k+1} + \vec{\beta}^k}{2}\right)\left[\vec{\alpha}^{k+1} - \vec{\alpha}^k\right] + \left(A + \frac{\Delta t}{2} B_2\left(\frac{\vec{\gamma}^{*k+1} + \vec{\gamma}^k}{2}\right)\right)\left[\vec{\beta}^{k+1} - \vec{\beta}^k\right]$$

$$= 2n\Delta t C\left(\frac{\vec{\beta}^{*k+1} + \vec{\beta}^k}{2}\right)\vec{\alpha}^k - \Delta t B_2\left(\frac{\vec{\gamma}^{*k+1} + \vec{\gamma}^k}{2}\right)\vec{\beta}^k ,$$

and

$$A\left[\vec{\alpha}^{k+1} - \vec{\alpha}^k\right] - B_3\left[\vec{\gamma}^{k+1} - \vec{\gamma}^k\right] = 2B_3\vec{\gamma}^k - 2A\vec{\alpha}^k .$$

The predictor-corrector scheme requires the solution of two sparse 3N x 3N linear algebraic systems for each step. It should be noted that all the matrices generated from nonlinear terms must be re-evaluated each time but because of their tridiagonal nature this should not be a major computational effort.

The Galerkin method has transformed the original partial differential equations into a system of ordinary differential equations in the coefficients of the basis functions. In fact, there is one ordinary differential equation associated with each basis function, V_i, for i = 1, ..., n. It is convenient to adjust or replace those ordinary differential equations that lie at the left-hand end ($\eta = \eta_1$) and the right-hand end ($\eta = \eta_N$) so that the boundary conditions are satisified. For the boundary conditions (2d, e), we would have that

$$\alpha_1(t) = 0 \quad , \qquad \gamma_1(t) = h_1(t) \ ,$$

$$(V_1 - K(t)V_1')\beta_1 - K(t)V_2'\beta_2 \Big|_{\eta=\eta_1} = 0 \ ,$$

$$\alpha_N(t) = 0 \quad \text{and} \quad \beta_N(t) = 1.$$

The initial conditions given by (2c) must also be satisfied. Two common procedures may be used to generate the initial values, i.e., to evaluate coefficients $\vec{\alpha}(0)$, $\vec{\beta}(0)$ and $\vec{\gamma}(0)$. The first is the least squares method, e.g., for $\vec{\beta}(0)$, we would have to solve for $\vec{\beta}(0)$ from

$$\sum_{i=1}^{N} \beta_i(0) \int_0^{\delta_\eta} V_i V_j \, d\eta = \int_0^{\delta_\eta} V_j \, d\eta \ , \quad j = 1, \cdots, N.$$

The second approach is to determine the value of the coefficients directlv. For example $\vec{\beta}(0)$ is found by solving the system

$$\sum_{i=1}^{N} \beta_i(0) V_i = 1.$$

By choosing $\eta = \eta_j$, j = 1 . . ., N and noting that the chapeau functions

$$V_i(\eta_j) = \begin{cases} 1, & 1 = j \\ 0, & i \neq j \end{cases},$$

gives $\beta_i(0) = 1$, i = 1, . . ., N. Even for non-smooth initial conditions the latter method works well provided N is large.

One advantage with the Galerkin method is that it yields a solution continuous in the space variable η for a specified time t = T. Thus it is convenient to solve equation (2b)

$$H' = F$$

by direct integration, as opposed to forming the variational problem, i.e.,

$$H(\eta_j, t) = \sum_{i=1}^{j} \alpha_i \int_0^{\eta_j} V_i(\eta) d\eta + h_1(t),$$

provided F is obtained as described above. This procedure is more efficient and just as accurate as the method described by (A2), the variational approach.

The validity and accuracy of the Galerkin method can be tested once the steady-state is achieved by comparisons against known steady-state solutions, for example, that due to Kuo (1971).

REFERENCES

Ames, W. F., 1969: Numerical Methods for Partial Differential Equations. Barnes and Noble, Inc., 291 pp.

Benton, E. R., 1966: On the flow due to a rotating disk. J. Fluid Mech., 24, 781-800.

Bode, L., L. M. Leslie, and R. K. Smith, 1975: A numerical study of boundary effects on concentrated vortices with application to tornadoes and watersprouts. Q. J. Roy. Met. Soc., 101, 313-324.

Boedewadt, von U. T., 1940: Die Drehatrömung über festem Grande. Z. angew. Math. Mech., 20, 241-253.

Brandes, E. A., 1977: Flow in severe thunderstorms observed by dual-doppler radar. Mon. Wea. Rev., 105, 113-120.

Ciarlet, P. G., M. H. Schultz, and R. S. Varga, 1967: Numerical methods of high-order accuracy for nonlinear boundary value problems. Numerische Mathematik, 9, 394-430.

Debnath, L., and S. Mukherjee, 1974: Inertial oscillations and multiple boundary layers in an unsteady rotating flow. Phys. Fluids, 17, 1372-1375.

Douglas, J., Jr., and T. Dupont, 1970: Galerkin methods for parabolic problems. SIAM J. on Numerical Analysis, 7, 575-625.

Florent, P., N. D. Nguyen, and N. D. Vo, 1973: Ecoulement instationnaire entre desques coaxiaux. J. Mécanious, 12. 555.

Greenspan, H. P., and L. N. Howard, 1963: On the time-dependent motion of a rotating fluid. J. Fluid Mech, 17, 385-404.

Karman, von T., 1921: Über laminare und turbulente Reibung. Z. angew. Math. Mech., 1, 233-252.

Kuo, H. L., 1971: Axisymmetric flow in the boundary layer of a maintained vortex. J. Atmos. Sci., 28, 20-41.

Pearson, C. E., 1965: Numerical solutions for the time-dependent viscous flow between two rotating coaxial disks. J. Fluid Mech., 21, 623-633.

Swartz, B., and B. Wendroff, 1974: The relative efficiency of finite difference and finite element methods, I: Hyperbolic problems and splines. SIAM J. on Numerical Analysis, 11, 979-993.

Taylor, G. I., 1915: Eddy motion in the atmosphere. Phil. Trans. Roy. Soc. London, A215, 1-26.

Thiriot, K. H., 1940: Grenzschlichtströmung kurz nach dem plötzlichen Anlauf bzw. Abstoppen eines rotierenden Bodens. A. angew. Math. Mech., 20, 1-13.

Thiriot, K. H., 1942: Untersuchungen über die Grenzschist einer Flüssigkeit über einer rotierenden Scheibe bei kleiner Winkelgeschwindigkeitsanderung. Z. angew. Math. Mech., 22, 23-28.

Thiriot, K. H., 1950: Grenzschlichtströmung kurz nach dem plötzlichen Anlauf bzw. Abstoppen eines rotierenden Bodens. Z. angew. Math. Mech., 30, 390-393.

Wang, H., P. Halpern, J. Douglas, Jr., and T. Dupont, 1972: Numerical solutions of the one-dimensional primitive equations using Galerkin approximations with localized basis functions. Mon. Wea. Rev., 100, 738-746.

List of Tables

Table 1

A comparison of the selected values of F, G and H computed at T = 56 and the corresponding quantities for steady-state conditions according to Kuo (1971). Other relevant quantities are n = 1.0, K = 5 exp(-T/5) $\simeq$ 0, h = 0.15 and Δt = 0.04.

	F		G		H	
		(Kuo's)		(Kuo's)		(Kuo's)
1.5	.45202	.44965	1.01321	1.01340	.55105	.54937
3.0	.03787	.03604	1.27417	1.27138	.93022	.92476
4.5	-.13811	-.13708	1.06660	1.06392	.80566	.79971
6.0	-.05143	-.04987	.94330	.94272	.65085	.64723
7.5	.02178	.02231	.96923	.96930	.63968	.63763
9.0	.01759	.01785	1.00820	1.00778	.67545	.67384
10.5	-.00253	-.00182	1.01040	1.00989	.68534	.68445
12.0	-.00613	-.00516	1.00035	1.00027	.67686	.67729
13.5	-.00159	-.00074	.99713	.99746	.67096	.67279
15.0	.00056	.00118	.99879	.99933	.67068	.67361

Table 2

Values of G and F for different time step, $\triangle t$, sizes. To conserve space only those values at T = 1.6 and select values of G and F are shown. Other relevant quantities are h = 0.15, n = 0.5 and K = exp(-T).

η	$\triangle t$ = .02	$\triangle t$ = .04	$\triangle t$ = .08
		values of G	
.0	.11541	.11556	.11586
		values of F	
.15	.09760	.09734	.09682
.30	.17478	.17427	.17323
.60	.27636	.27535	.27332
1.50	.30988	.30773	.30340
3.00	.11475	.11275	.10877
6.00	.00143	.00136	.00124
12.00	.00000	.00000	.00000

Table 3

Same as Table 2 but for T = 8.0

η	$\Delta t = .02$	$\Delta t = .04$	$\Delta t = .08$
		values of G	
.0	.00015	.00015	.00015
		values of F	
.15	.16911	.16909	.16907
.30	.31641	.31638	.31633
.60	.55126	.55112	.55112
1.50	.90641	.90629	.90604
3.00	.91307	.91281	.91225
6.00	.24816	.24765	.24658
12.00	-.68194	-.68080	-.67834

Table 4

Same as Table 3 except $K = 5 \exp(-T/5)$, $\Delta t = 0.04$ and for different h's as shown

η	h = .075	h = .15	h = .30
	values of G		
.0	.42270	.42058	.41527
	values of F		
.3	.15147	.15235	.15451
.6	.24253	.24410	.24804
1.2	.29887	.30126	.30729
2.4	.18766	.18985	.19543
4.8	-.01220	-.01288	-.01376
9.6	.00660	.00609	.00596
15.0	.00000	.00006	-.00002

List of Figures

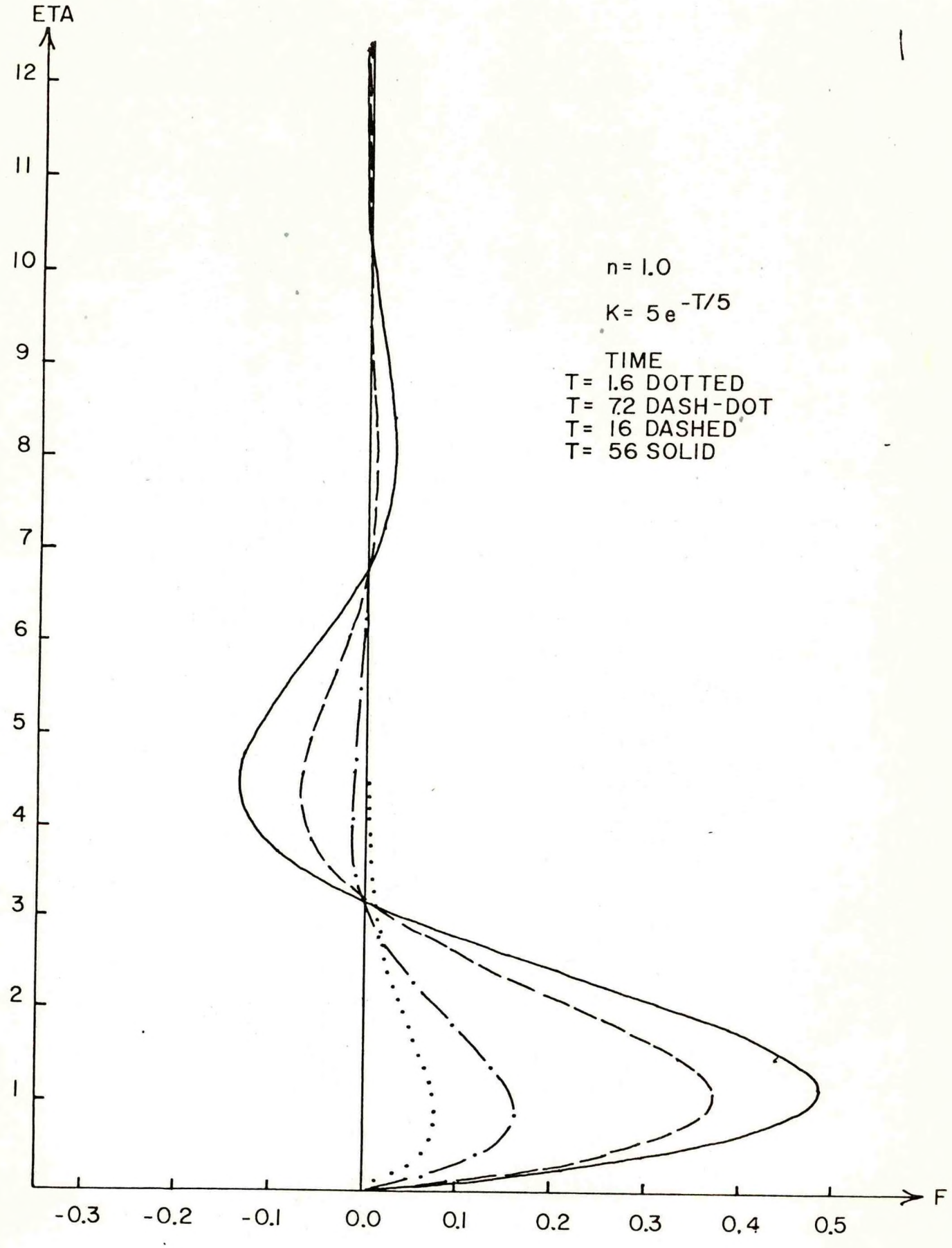
ETA
12
11
10
9
8
7
6
5
4
3
2
1
n = 1.0
K = 5e^-T/5
TIME
T = 1.6 DOTTED
T = 7.2 DASH-DOT
T = 16 DASHED
T = 56 SOLID
-0.3
-0.2
-0.1
0.0
0.1
0.2
0.3
0.4
0.5
F

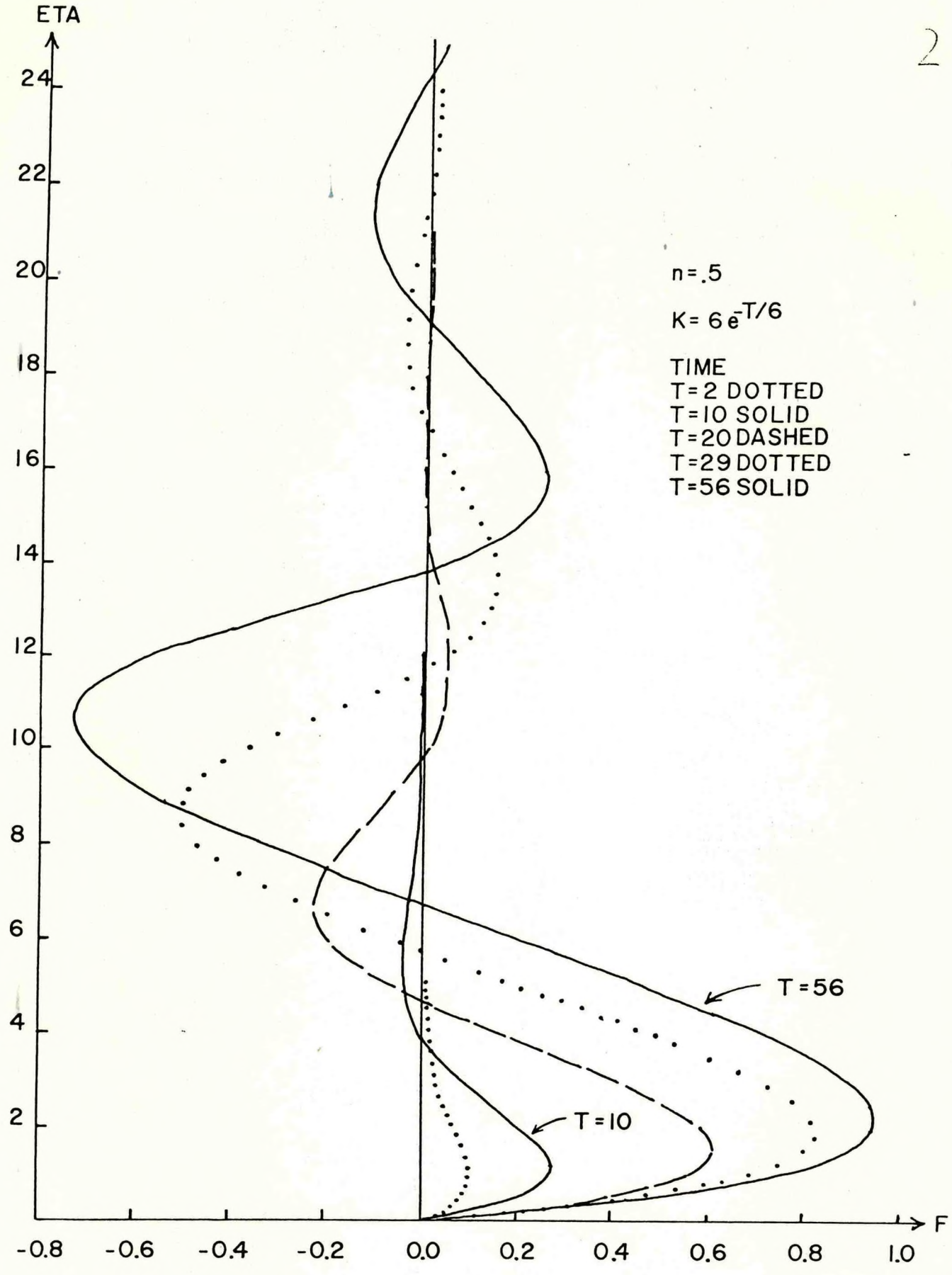
ETA
24
22
20
18
16
14
12
10
8
6
4
2
n=.5
K= 6e^-T/6
TIME
T=2 DOTTED
T=10 SOLID
T=20 DASHED
T=29 DOTTED
T=56 SOLID
T=56
T=10
-0.8
-0.6
-0.4
-0.2
0.0
0.2
0.4
0.6
0.8
1.0
F

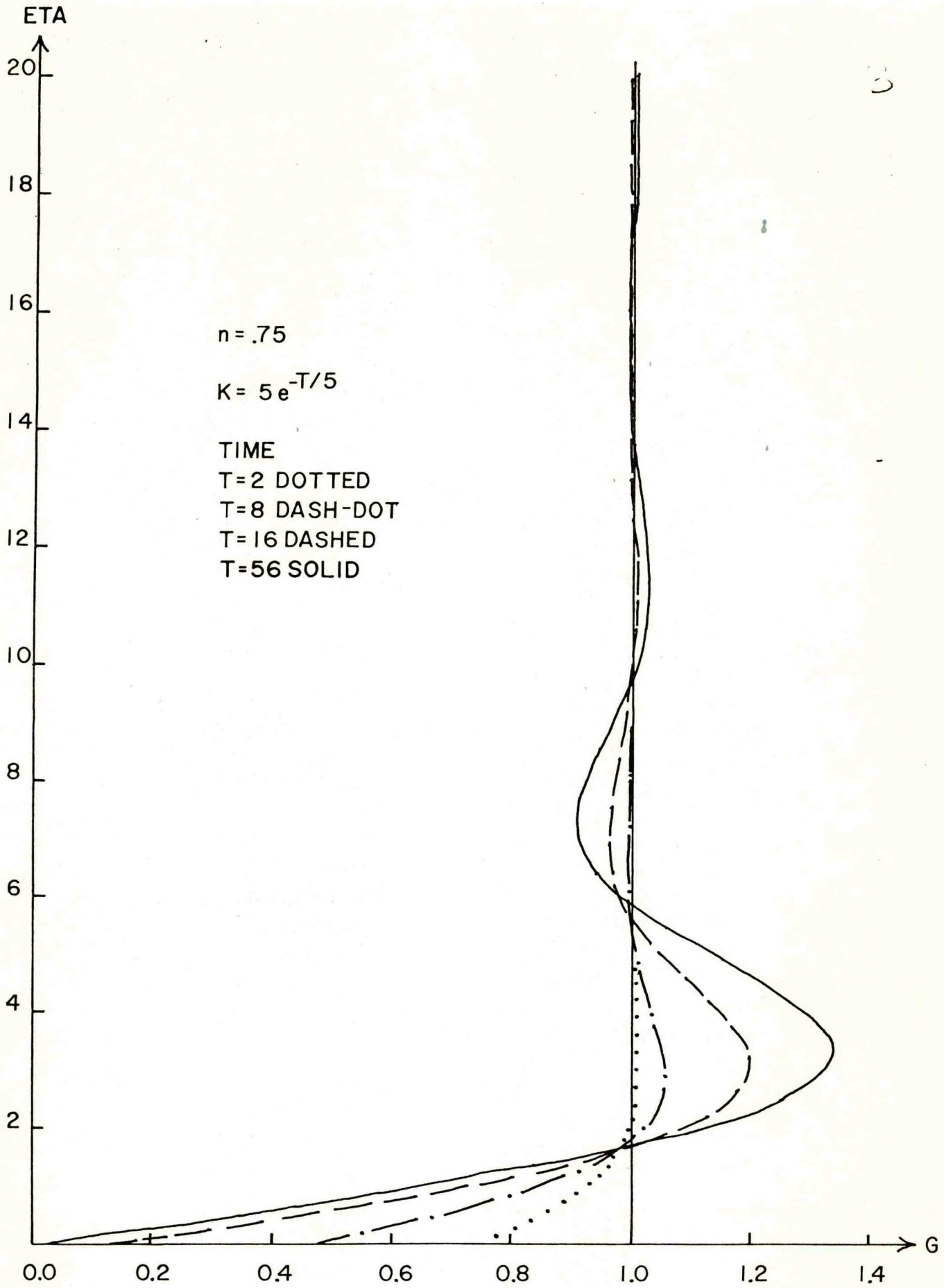
ETA
20
18
16
14
12
10
8
6
4
2
n = .75
K = 5 e^-T/5
TIME
T=2 DOTTED
T=8 DASH-DOT
T=16 DASHED
T=56 SOLID
0.0
0.2
0.4
0.6
0.8
1.0
1.2
1.4
G

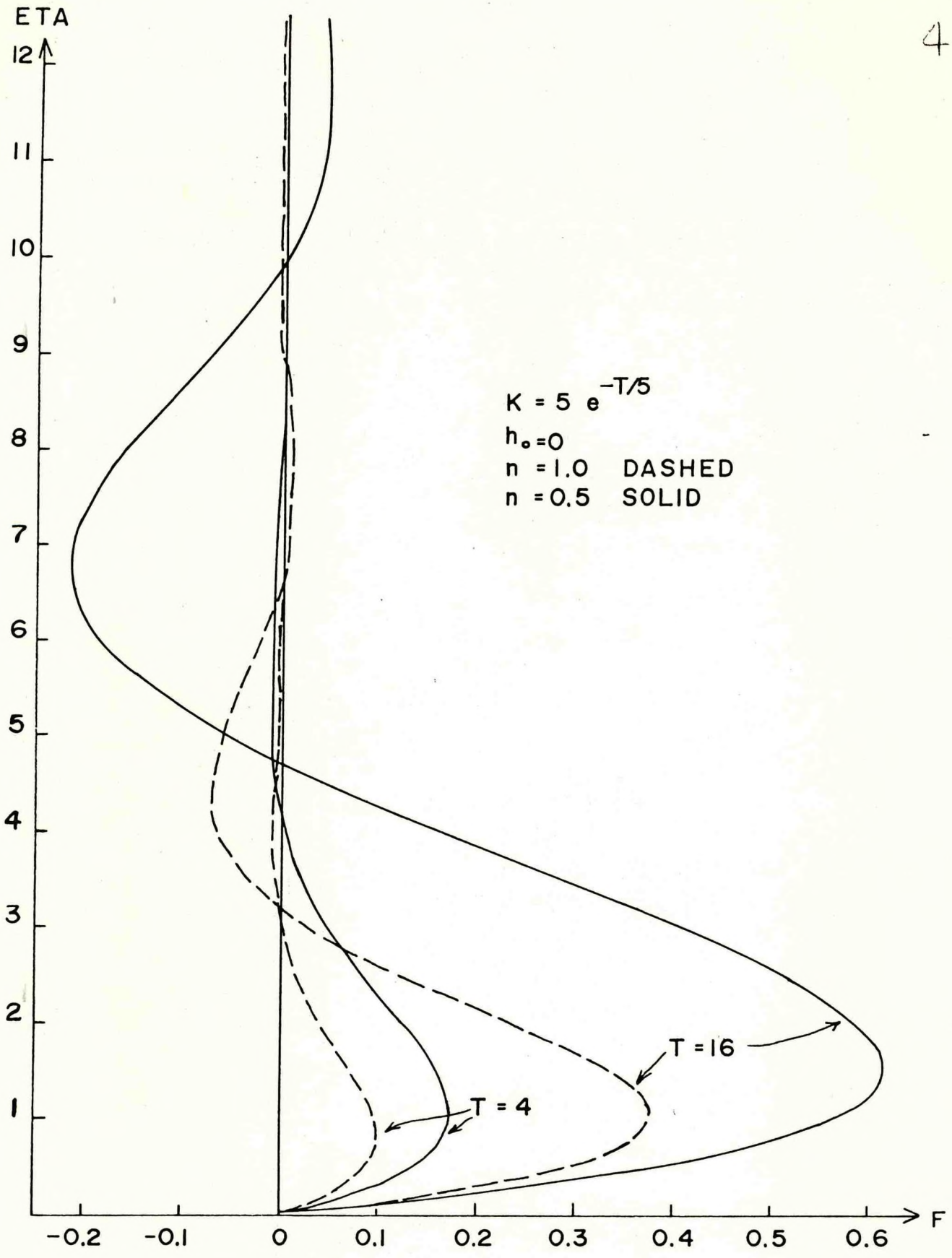
ETA
12
11
10
9
8
7
6
5
4
3
2
1
K = 5 e^-T/5
h₀ = 0
n = 1.0 DASHED
n = 0.5 SOLID
T = 16
T = 4
-0.2
-0.1
0
0.1
0.2
0.3
0.4
0.5
0.6
F

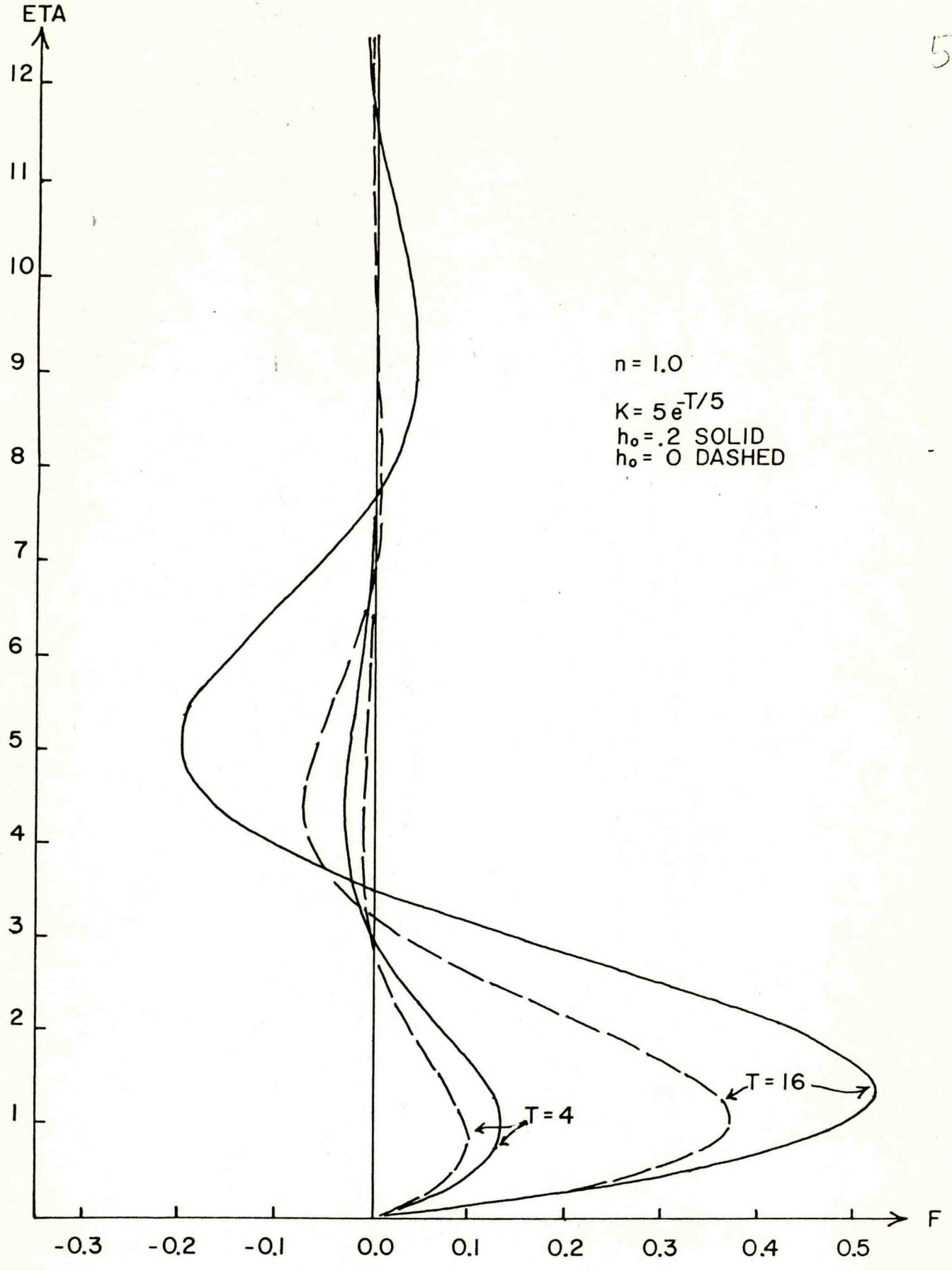
ETA
12
11
10
9
8
7
6
5
4
3
2
1
n = 1.0
K = 5e^-T/5
h₀ = .2 SOLID
h₀ = 0 DASHED
T = 16
T = 4
-0.3
-0.2
-0.1
0.0
0.1
0.2
0.3
0.4
0.5
F

VERTICAL VELOCITY (H) AT THE TOP OF THE BOUNDARY LAYER

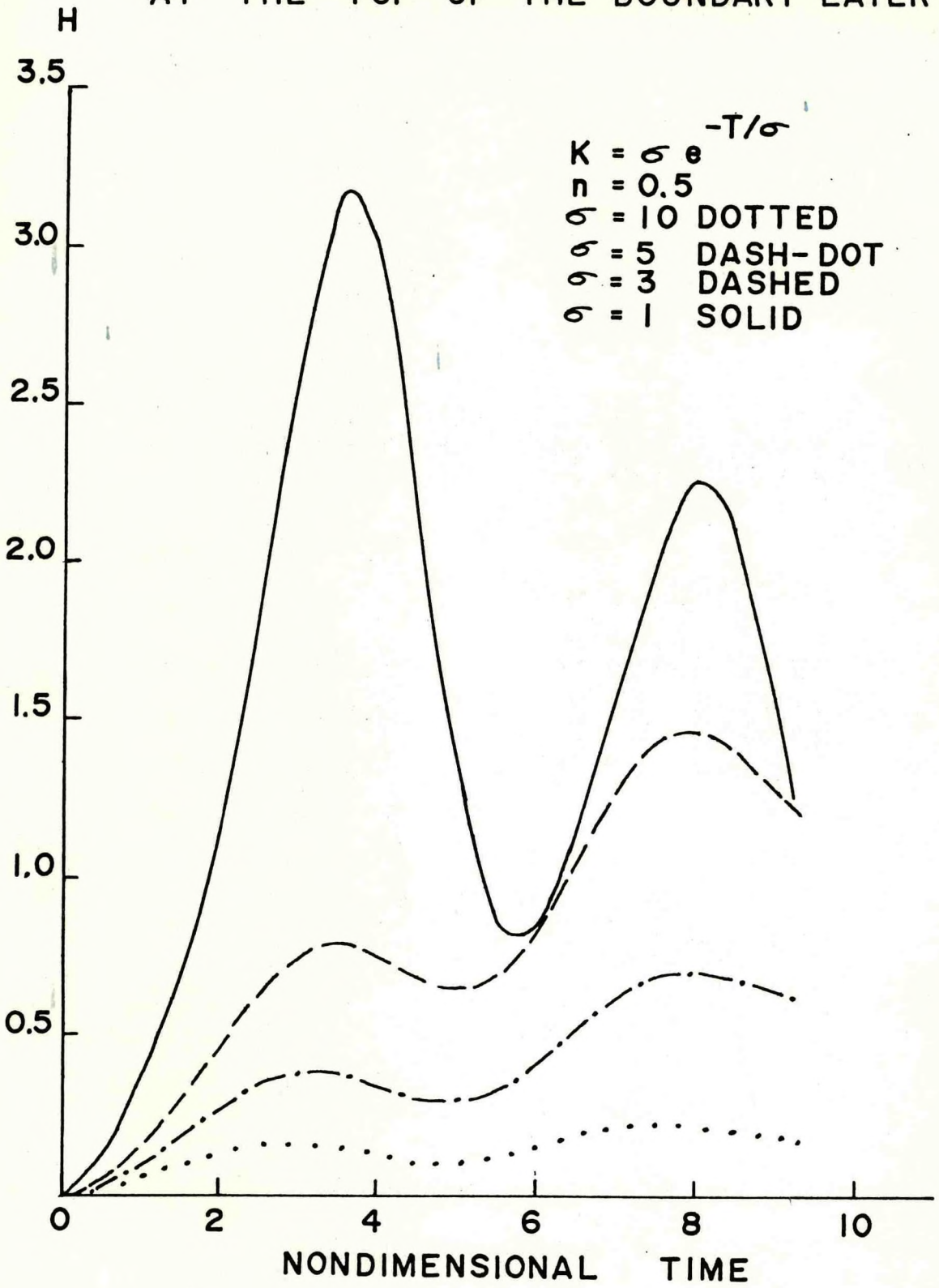

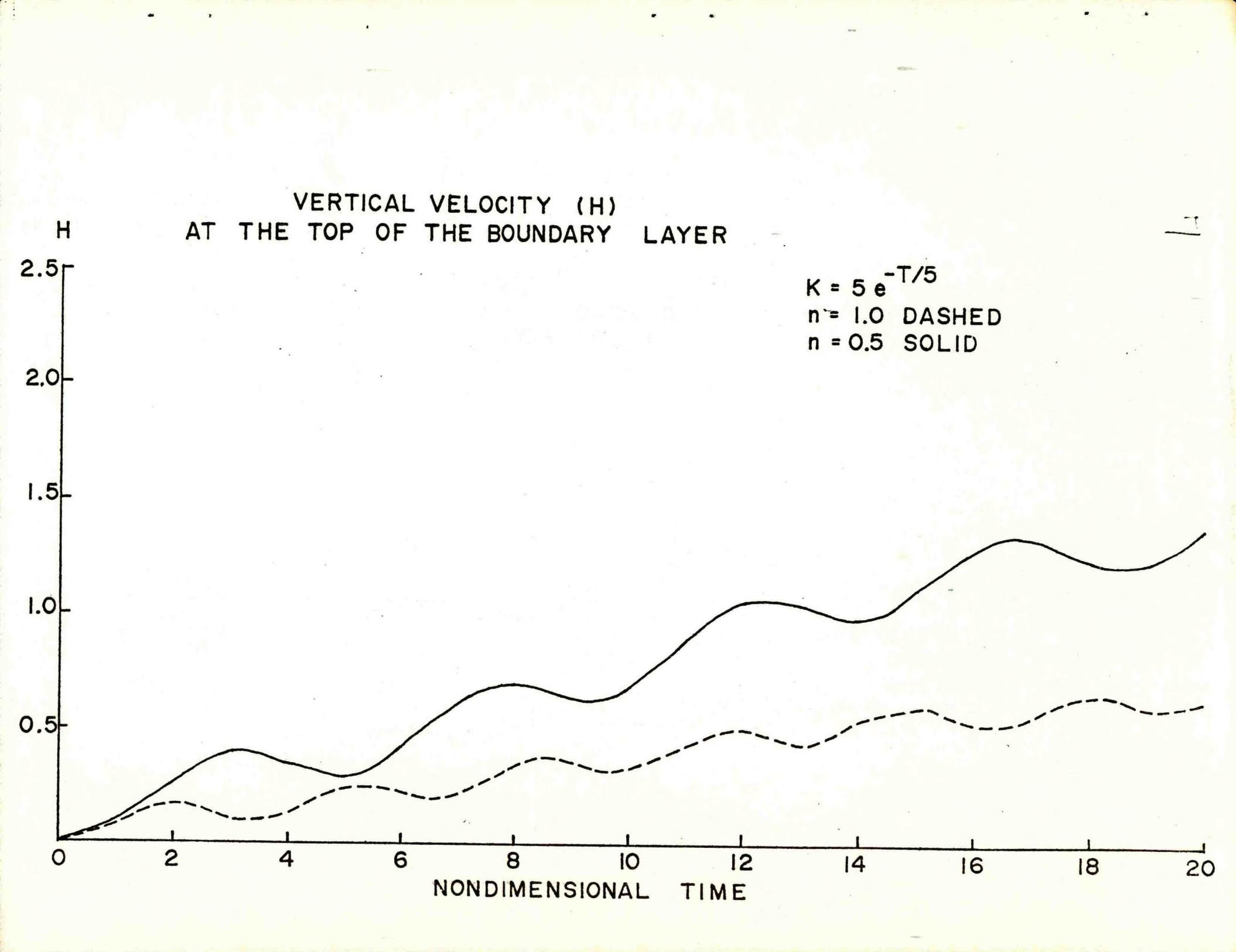
VERTICAL VELOCITY (H)
AT THE TOP OF THE BOUNDARY LAYER
H
2.5
2.0
1.5
1.0
0.5
K = 5 e^-T/5
n = 1.0 DASHED
n = 0.5 SOLID
0
2
4
6
8
10
12
14
16
18
20
NONDIMENSIONAL TIME

DEPTH OF SURFACE INFLOW LAYER AS A FUNCTION OF n

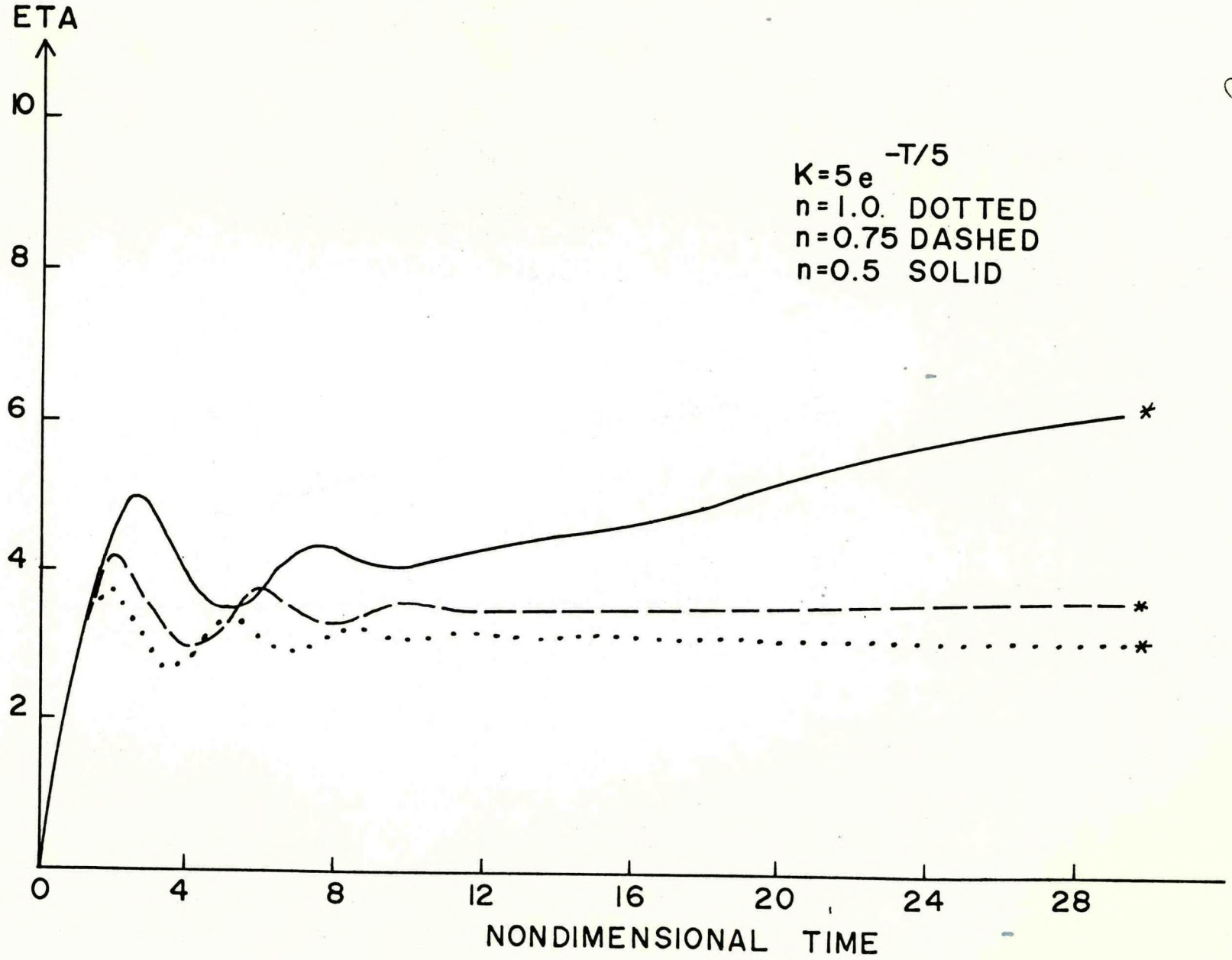

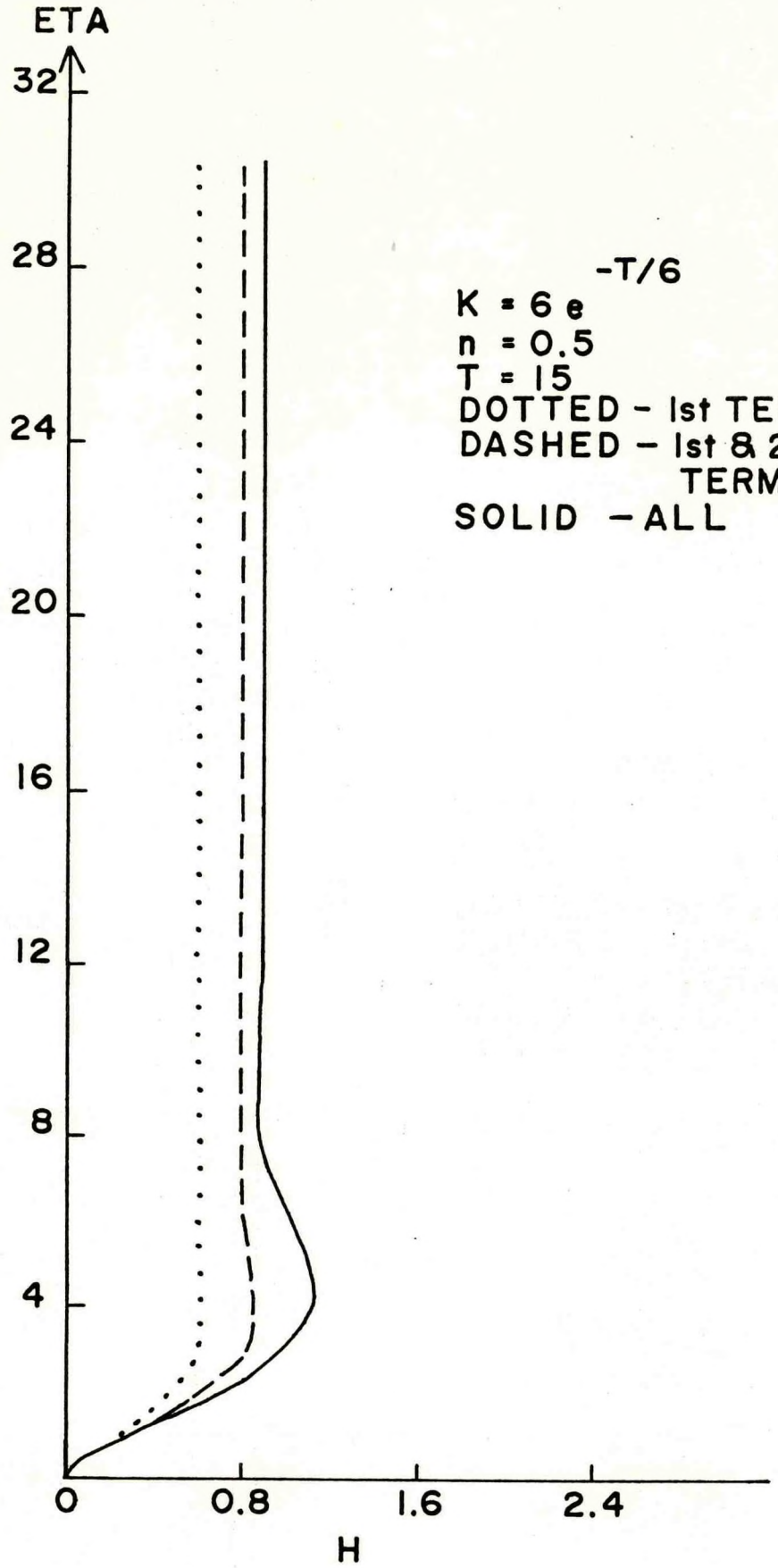
ETA
32
28
24
20
16
12
8
4
0
0.8
1.6
2.4
H
-T/6
K = 6 e
n = 0.5
T = 15
DOTTED - 1st TERM
DASHED - 1st & 2nd TERMS
SOLID - ALL

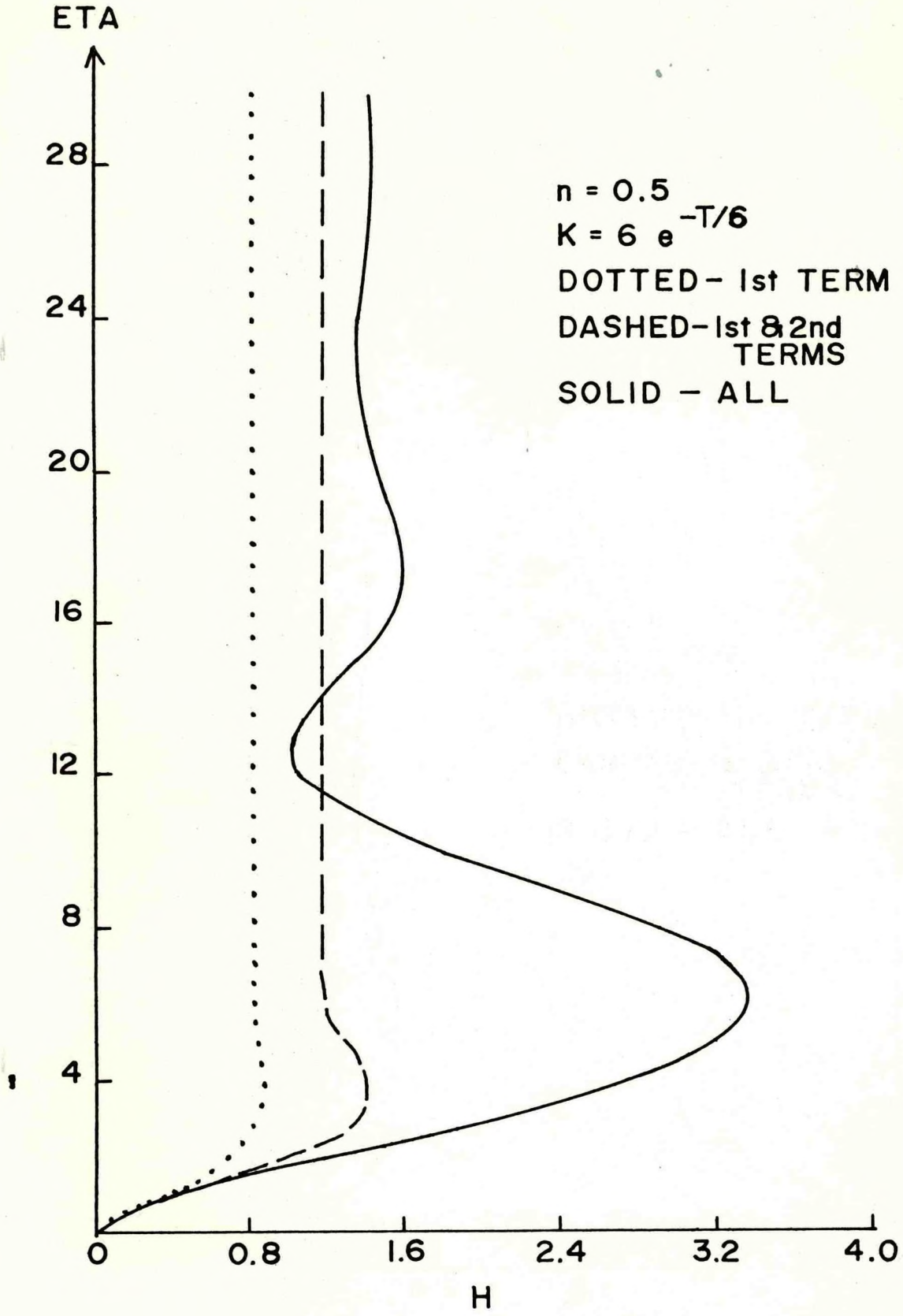
ETA
28
24
20
16
12
8
4
0
0.8
1.6
2.4
3.2
4.0
H
n = 0.5
K = 6 e^-T/6
DOTTED - 1st TERM
DASHED - 1st & 2nd TERMS
SOLID - ALL